Lower oceanic δ^{13}C during the Last Interglacial compared to the Holocene

Shannon A. Bengtson[1,2], Laurie C. Menviel[1], Katrin J. Meissner[1,2], Lise Missiaen[1], Carlye D. Peterson[3], Lorraine E. Lisiecki[4], and Fortunat Joos[5,6]

[1]Climate Change Research Centre, The University of New South Wales, Sydney, Australia
[2]The Australian Research Council Centre of Excellence for Climate Extremes, Australia
[3]Earth Sciences, University of California, Riverside, California, USA
[4]Department of Earth Science, University of California, Santa Barbara, California, USA
[5]Climate and Environmental Physics, Physics Institute, University of Bern, Bern, Switzerland
[6]Oeschger Centre for Climate Change Research, University of Bern, Bern, Switzerland

Correspondence: Shannon A. Bengtson (s.bengtson@unsw.edu.au)

Abstract.

The last time in Earth's history when the high latitudes were warmer than during pre-industrial times was the last interglacial (LIG, 129–116 ka BP). Since the LIG is the most recent and best documented warm time period, it can provide insights into climate processes in a warmer world. However, some key features of the LIG are not well constrained, notably the oceanic circulation and the global carbon cycle. Here, we use a new database of LIG benthic δ^{13}C to investigate these two aspects.

5   We find that the oceanic mean δ^{13}C was ∼0.2 ‰ lower during the LIG (here defined as 125–120 ka BP) when compared to the mid-Holocene (7–4 ka BP). As the LIG was slightly warmer than the Holocene, it is possible that terrestrial carbon was lower, which would have led to both a lower oceanic δ^{13}C and atmospheric δ^{13}CO$_2$ as observed in paleo-records. However, given the multi-millennial timescale, the lower oceanic δ^{13}C most likely reflects a long-term imbalance between weathering and burial of carbon. The δ^{13}C distribution in the Atlantic Ocean suggests no significant difference in the latitudinal and depth

10   extent of North Atlantic Deep Water (NADW) between the LIG and the mid-Holocene. Furthermore, the data suggests that the multi-millennial mean NADW transport was similar between these two time periods.

1   Introduction

The most recent and well documented warm time period, the last interglacial (LIG), began at the end of the penultimate

15   deglaciation (∼129 thousand years before present, ka BP hereafter) and ended with the last glacial inception (∼116 ka BP) (Govin et al., 2015; Brewer et al., 2008; Dutton and Lambeck, 2012; Masson-Delmotte et al., 2013). The LIG was globally somewhat warmer than pre-industrial (PI, ∼1850–1900 (IPCC, 2013), Shackleton et al. (2020)); PI is estimated to be cooler by ∼0.7 °C than the peak of the Holocene (∼5 ka BP) (Marcott et al., 2013). Though not an exact analogue for future warming, the LIG may still help shed light on future climates. In particular, we seek to constrain the mean LIG ocean circulation and

20   estimate the global oceanic mean δ^{13}C.

1.1 Climate during the Last Interglacial

As greenhouse gas concentrations were comparable to the Holocene, the LIG was most likely relatively warm because of the high boreal summer insolation (Laskar et al., 2004). During the LIG, the atmospheric CO_2 concentration was relatively stable around ∼280 p.p.m. (Bereiter et al., 2015; Lüthi et al., 2008), while during the Holocene CO_2 first decreased by about 5 p.p.m.

25 starting at 11.7 ka BP before increasing by ∼28 p.p.m. until reaching a mean of 279 p.p.m. at ∼2 ka BP (Fig. 1a) (Eggleston et al., 2016b). Additionally, during the LIG and the Holocene, N_2O peaked at around ∼267 p.p.b (Spahni et al., 2005; Flückiger et al., 2002), while CH_4 reached ∼700 p.p.b (Petit et al., 1999) and ∼675 p.p.b respectively (Flückiger et al., 2002). Ice core data indicate strong polar warming in Greenland that was 8.5±2.5 °C higher during the peak of the LIG compared to PI (Landais et al., 2016). Similarly, EPICA DOME C record suggests that the highest Antarctic temperatures from the last 800 ka

30 occurred during the LIG (Masson-Delmotte et al., 2010) (Fig. 1b). Global sea-level was 6–9 m higher at the LIG compared to PI (Dutton et al., 2015; Kopp et al., 2009), thus indicating significant ice-mass loss from both Antarctica and Greenland.

Strong polar warming is also supported by terrestrial and marine temperature reconstructions. On land, proxy records from mid to high latitudes indicate higher temperatures during the LIG compared to PI, particularly in North America (Anderson et al., 2014; Montero-Serrano et al., 2011; Axford et al., 2011). In Alaska and Northern Europe, summer temperatures were

35 higher by about 1–2 °C (Kaspar et al., 2005), though some Northern European records indicate a smaller temperature increase of up to 1 °C (Plikk et al., 2019), and there is some inconsistency in the European temperature records (Otto-Bliesner et al., 2020). Sea surface temperature (SST) reconstructions also indicate higher temperatures at the LIG compared to PI (e.g. the Mediterranean record in Fig. 1c). A global analysis of SST records suggests that the surface ocean was 0.5±0.3 °C higher during the LIG compared to 1870–1889, with the largest increases occurring at high latitudes (Hoffman et al., 2017). Another

40 global reconstruction estimates that the global mean SST was 0.7±0.6 °C higher during the LIG compared to peak Holocene temperatures (McKay et al., 2011). During boreal summer, temperatures in the Arctic were likely 4–5 °C higher with reduced Arctic summer sea ice extent (Stein et al., 2017). Temperatures of surface waters off Greenland were likely 3–5 °C higher during the early to mid-LIG compared to the warmest period of the Holocene (Irvalı et al., 2012). North Atlantic summer SSTs were on average 1.1 °C higher than PI, while Southern Ocean austral summer SSTs are estimated to have been about 1.8 °C

45 higher at 127 ka BP than PI (Capron et al., 2017).

Polar warming was also associated with significant changes in vegetation. Pollen records suggest a contraction of tundra and an expansion of boreal forests across the Arctic (CAPE, 2006), in Russia (Tarasov et al., 2005), and in North America (Muhs et al., 2001; de Vernal and Hillaire-Marcel, 2008; Govin et al., 2015). The few Saharan records suggest a green Sahara period during the LIG (Larrasoaña et al., 2013; Drake et al., 2011), consistent with a stronger West African monsoon (Otto-Bliesner

50 et al., 2020). Although these reconstructions indicate changes in vegetation distribution during the LIG, the total amount of carbon stored on land remains poorly constrained.

Recent numerical experiments of the LIG as part of the Paleomodel Intercomparison Project Phase 4 (PMIP4) simulate significant warming over Alaska and Siberia in boreal summer, with mean annual temperature anomalies of close to zero, which is in good agreement with the proxy record (Otto-Bliesner et al., 2020). Despite this and other recent data compilations
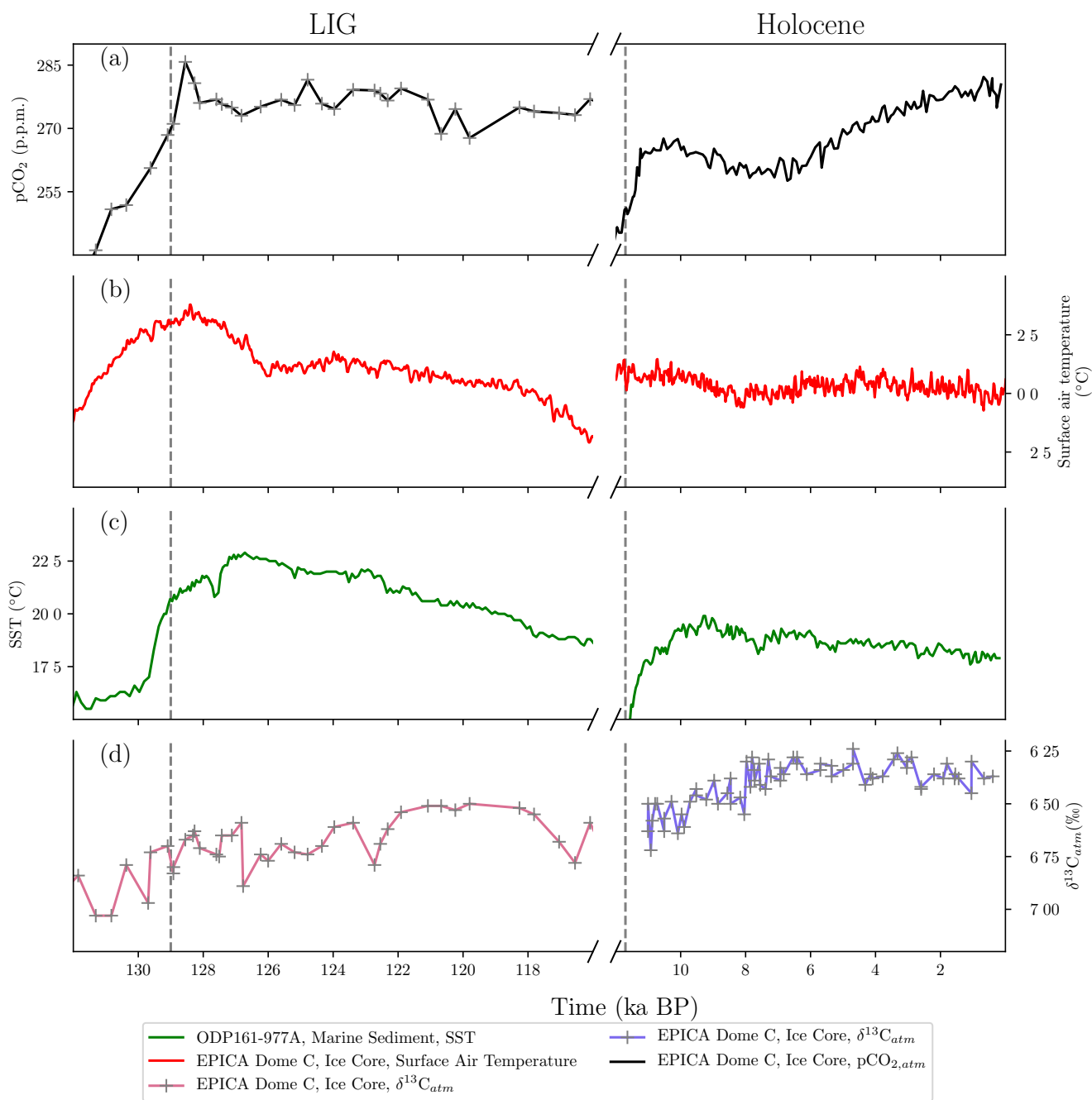
Figure 1. LIG and Holocene timeseries of a) EPICA Dome C ice core $pCO_{2,atm}$ (Schneider et al., 2013; Eggleston et al., 2016a), b) EPICA Dome C ice core surface air temperatures determined from deuterium measurements (Jouzel and Masson-Delmotte, 2007), c) sea surface temperatures (SST) determined from alkenones and oxygen isotopes from the Mediterranean marine sediment core ODP161-977A (Martrat et al., 2004), and d) EPICA Dome C ice core $\delta^{13}C_{atm}$ (Elsig et al., 2009; Schneider et al., 2013). Grey vertical dotted lines indicate the commencement of the LIG and Holocene periods.

55 and modelling efforts (including Bakker et al. (2013)), to date there are many open questions remaining about the LIG. In particular, stronger constraints are needed on the extent of Greenland and Antarctic ice sheets, on ocean circulation and the global carbon cycle.

1.2 Atlantic Meridional Overturning Circulation during the Last Interglacial

It is important to constrain the state of the Atlantic Meridional Overturning Circulation (AMOC) at the LIG given its significant
60 role in modulating climate. Seven coupled climate models integrated with transient 130–115 ka BP boundary conditions simulate different AMOC trends, with some models producing a strengthening of the AMOC while others compute a weakening during the LIG (Bakker et al., 2013). Paleoproxy records suggest equally strong and deep North Atlantic Deep Water (NADW) during the LIG and the Holocene (e.g. Böhm et al., 2015; Lototskaya and Ganssen, 1999), with possible southward expansion of the Arctic front related to changes in the strength of the subpolar gyre (Mokeddem et al., 2014), and AMOC weakening
65 during a few multi centennial-scale events between 127 and 115 ka BP (e.g. Galaasen et al., 2014b; Mokeddem et al., 2014; Tzedakis et al., 2018; Lehman et al., 2002; Helmens et al., 2015; Oppo et al., 2006; Rowe et al., 2019).

1.3 Oceanic δ^{13}C and the carbon cycle

Stable carbon isotopes are a powerful tool for investigating ocean circulation (e.g. Curry and Oppo, 2005; Eide et al., 2017) and the global carbon cycle (e.g. Menviel et al., 2017; Peterson et al., 2014). Since the largest carbon isotope fractionation occurs
70 during photosynthesis, organic matter is enriched in ^{12}C (low δ^{13}C), while atmospheric CO_2 and surface water dissolved inorganic carbon (DIC) become enriched in ^{13}C (high δ^{13}C). On land, the different photosynthetic pathways (which differentiate C3 and C4 plants) fractionate carbon differently, producing typical signatures of about -37 to -20 ‰ for C3 plants (Kohn, 2010) and around -13 ‰ for C4 plants (Basu et al., 2015), though these values vary with a number of factors including precipitation, atmospheric CO_2 concentration and δ^{13}C, light, nutrient availability, and plant species (Diefendorf et al., 2010; Farquhar
75 et al., 1989; Schubert and Jahren, 2012; Cernusak et al., 2013; Leavitt, 1992; Diefendorf and Freimuth, 2017; Farquhar, 1983; Keller et al., 2017). In the ocean, phytoplankton using the C3 photosynthetic pathway are found to have fractionation during photosynthesis that depends on the concentration of dissolved CO_2. Thus, atmospheric $\delta^{13}CO_2$ during the LIG (Fig. 1d) is influenced by plant type, the cycling of organic carbon within the ocean, the total amount of carbon in vegetation and soils, temperature-dependent air-sea flux fractionation (Zhang et al., 1995; Lynch-Stieglitz et al., 1995), and, on longer time scales,
80 by interactions with the lithosphere. Today, the mean surface DIC is thereby enriched by ∼8.5 ‰ compared to the atmosphere due to fractionation during air-sea gas exchange (Schmittner et al., 2013; Menviel et al., 2015).

NADW is characterised by low nutrients and high δ^{13}C as a result of a high nutrient and carbon utilisation by marine biota and fractionation during air-sea gas exchange in the northern North Atlantic. Along its path through the Atlantic basin interior, organic matter remineralisation lowers δ^{13}C, reducing δ^{13}C to ∼0 ‰ by the time these water masses reach the Southern Ocean.
85 Conversely, Antarctic Bottom Water (AABW) has a high nutrient content and low δ^{13}C.

The tight relationship between the water masses apparent oxygen utilisation, nutrient content and δ^{13}C has revealed the potential of δ^{13}C as a water mass ventilation tracer (Eide et al., 2017). The δ^{13}C of benthic foraminifera shells, particularly

of the species *Cibicides wuellerstorfi*, has been found to reliably represent the δ^{13}C signature of DIC (Belanger et al., 1981; Zahn et al., 1986; Duplessy et al., 1984) and has therefore been used to better constrain the extent of different water masses.

90 A δ^{13}C mass balance between the atmosphere, ocean and land has been previously used to constrain changes in terrestrial carbon between the Last Glacial Maximum ($\sim$20 ka BP) and Holocene. However, since on longer time scales the exchange of carbon with the lithosphere also influences the global mean δ^{13}C, it cannot be applied to evaluate terrestrial carbon changes between the LIG and Holocene. It has been estimated that the amount of carbon both entering and exiting the lithosphere due to weathering and burial of organic carbon fluxes could be from 0.274 to 0.344 Gt C yr^{-1} (Schneider et al., 2013), though

95 these vary through time (Hoogakker et al., 2006). Over timescales greater than 10 ka, the influence of weathering and burial of carbon might therefore dominate the δ^{13}C signal (Jeltsch-Thömmes et al., 2019; Jeltsch-Thömmes and Joos, 2020).

Here, we present a new compilation of benthic δ^{13}C from *Cibicides wuellestorfi* spanning the 130–118 ka BP time period. We use this data to compare the δ^{13}C signal of the LIG with that of the Holocene and to determine the difference in average ocean δ^{13}C between the two time periods. We then investigate the Atlantic Meridional Overturning Circulation (AMOC) during

100 the LIG with our new benthic δ^{13}C database. Finally, we qualitatively explore the role of the various processes affecting the δ^{13}C difference between the LIG and the Holocene.

2 Database and methods

2.1 Database

We present a new compilation of benthic δ^{13}C records covering the LIG (130–118 ka BP) and, for comparison, the mid-

105 Holocene period (8–2 ka BP). Our database only includes measurements on *Cibicides wuellerstorfi* as no significant fractionation between the calcite shells and the surrounding DIC has been measured in this species (Belanger et al., 1981; Zahn et al., 1986; Duplessy et al., 1984).

Our compilation is predominantly based on Lisiecki and Stern (2016) (53 cores), but includes 14 cores described in Oliver et al. (2010), as well as a few other records (CH69-K09 (Labeyrie et al., 2017), MD03-2664 (Galaasen et al., 2014a), MD95-

110 2042 (Govin, 2012), IODP 303-U1308 (Hodell et al., 2008), and ODP 1063 (Poirier and Billups, 2014)). The full core list and their respective locations is provided in the supplementary materials.

2.2 Age models

Due to the lack of absolute age markers, such as tephra layers, the LIG age models mostly rely on alignment strategies that tie each record to a well-dated reference record. The age model tie-points used in this study are taken from the original age

115 model publications. The reference records used by Lisiecki and Stern (2016) consist of eight regional stacks (one for the intermediate and one for the deep ocean for each the North Atlantic, South Atlantic, Pacific and Indian Oceans) of benthic δ^{18}O that were dated through alignment with other climatic archives such as ice-rafted debris records, synthetic ice core records and speleothems. The use of regional stacks, rather than a single global stack, improved stratigraphic alignment targets

and provided more robust age models. The estimated uncertainty for this group of cores is ± 2 ka. Please refer to Lisiecki and
120 Stern (2016) for further details. Oliver et al. (2010) defined their age tie points assuming that sea level minima and benthic $\delta^{18}O$
maxima are synchronous. The benthic $\delta^{18}O$ records were aligned with each other and then tied to the Dome Fuji chronology
(based on O_2/N_2) (Kawamura et al., 2007). Please refer to Shackleton et al. (2000) and Oliver et al. (2010) for an extensive
method description. The estimated age model uncertainty on this group of cores is estimated to range from ± 1 to ± 2.5 ka.

The age models for the additional cores were determined using similar alignment techniques: SSTs were correlated to
125 the NGRIP Greenland ice core for CH69-K09 and MD95-2042 (Govin et al., 2012). The age model for MD03-2664 was
determined by correlating MD03-2664 $\delta^{18}O$ with previously dated MD95-2042 $\delta^{18}O$ (Galaasen et al., 2014b). IODP 303-
U1308 $\delta^{18}O$ and ODP 1063 $\delta^{18}O$ were aligned to the LR04 stack (Lisiecki and Raymo, 2005).

The Holocene age models have been generally based on planktonic foraminifera radiocarbon dates (Waelbroeck et al., 2001;
Stern and Lisiecki, 2014), which have been converted into calendar ages using IntCal13 and reservoir ages based on modern
130 observations (Key et al., 2004), which are assumed to have remained fairly stable across the Holocene. The age uncertainty
associated with these Holocene radiocarbon-based age models is generally less than ± 0.5 ka. However, it is important to note
that Holocene age models from Oliver et al. (2010) were derived using the same method as their LIG age models, leading to
larger age uncertainties of about ± 1 - ± 2.5 ka for this set of Holocene records (14 cores).

The tie points were used to derive a full age-depth model assuming a constant sedimentation rate between tie-points (i.e.
135 linear interpolation).

2.3 Spatial coverage

The spatial distribution of the database for the Holocene and the LIG is shown in Fig. 2. There is more data in the Atlantic
Ocean (69 LIG, 113 Holocene) than in the Pacific (18 LIG, 19 Holocene) and Indian (4 LIG, 7 Holocene) Oceans. We used
this database to determine 1) if there is a significant difference in the average ocean $\delta^{13}C$ signal at the LIG compared to
140 the Holocene, and 2) if ocean circulation patterns were comparable. Due to the sparsity of data in the Indian and Pacific
Oceans, our investigation is primarily focused on the Atlantic. Additionally, the temporal uncertainties (~ 2 ka) do not permit
an investigation of centennial-scale events, and therefore we restrict our analysis to mean LIG and Holocene conditions.

3 Results

The $\delta^{13}C$ signal varies significantly regionally and with depth. The highest average $\delta^{13}C$ values are associated with NADW
145 and are generally found at intermediate depths ($\sim 1,500$–$3,000$ m) in the North Atlantic, with organic matter remineralisation
leading to a $\delta^{13}C$ decrease along the NADW path. The lowest $\delta^{13}C$ values are in the deep south Atlantic (>4,000 m) because
the AABW end member is much lower than its NADW counterpart. Since the Indian and Pacific Oceans are mostly ventilated
from southern-sourced water masses, $\delta^{13}C$ generally decreases northward in these two basins.

Since the number of cores is not consistent across the two time periods, and given the high regional variability observed
150 in $\delta^{13}C$, it is not possible to simply average all available data to determine the global mean $\delta^{13}C$. Furthermore, the spatial
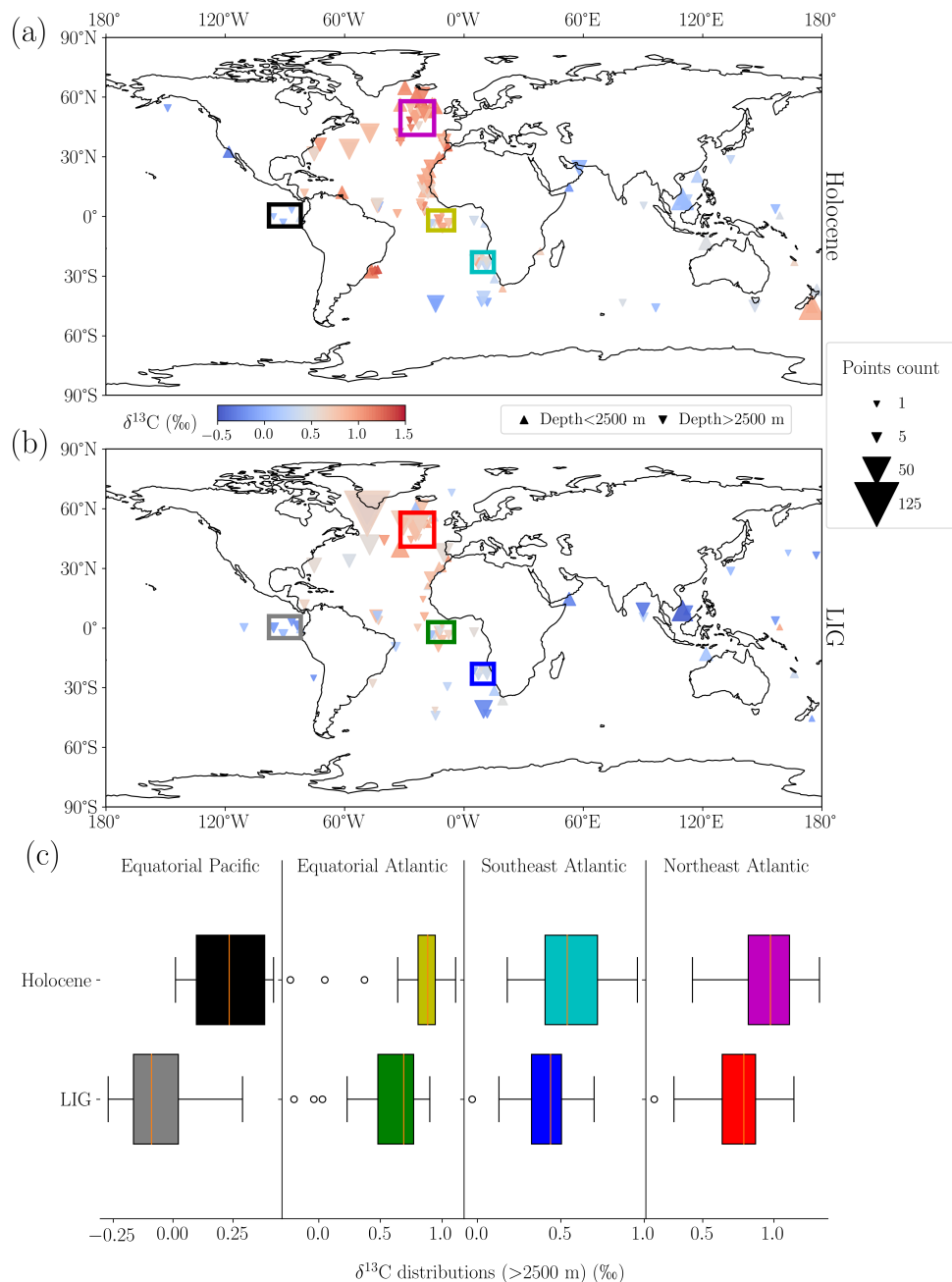
Figure 2. Global distribution of benthic foraminifera δ^{13}C covering the Holocene (8–2 ka BP) (a) and LIG (130–118 ka BP) (b). Symbol size indicates the number of values per core, colour indicates average δ^{13}C, and the triangle direction indicates the proxy depth (upward-pointing triangle: between 1,000 and 2,500 m depth, downward-pointing triangle: deeper than 2,500 m). Four specific regions are outlined: eastern equatorial Pacific (black, grey), equatorial Atlantic (yellow, green), southeast Atlantic (cyan, blue), and northeast Atlantic (magenta, red). Panel c: box plots for each region showing data below 2,500 m (box colours correspond to the region outline colours). Orange vertical lines show the median. The whiskers indicate the lower and upper fences of the data, and the clear circles are outliers.

Table 1. Regional summary of δ^{13}C below 2,500 m depth for the LIG (125–120 ka BP) and mid-Holocene (7–4 ka BP) using a single value per core for each time slice. Shown are the means (δ^{13}C, ‰), standard deviations (σ, ‰), and counts (N) for both time periods, along with the time period regional anomalies ($\Delta\delta^{13}$C, ‰) and p-values from two-sample t-tests between the two time periods.

| Region | Latitude | Longitude | Holocene | | | LIG | | | LIG | |
			δ^{13}C (‰)	σ (‰)	N	δ^{13}C (‰)	σ (‰)	N	$\Delta\delta^{13}$C (‰)	P value
Northeast Atlantic	41° N-58° N	15° E-32° E	0.91	0.21	28	0.76	0.12	29	-0.15	0.0017
Equatorial Atlantic	7° S-3° N	5° E-18° E	0.81	0.28	15	0.61	0.23	8	-0.19	0.0488
Southeast Atlantic	28° S-18° S	15° W-4° W	0.52	0.22	18	0.40	0.11	12	-0.13	0.0786
Eastern equatorial Pacific	5° S-6° N	82° E-98° E	0.07	0.04	3	-0.11	0.10	8	-0.18	0.0204

heterogeneity of the data density adds to the complexity of the problem. To address these points, we first analyse differences between the LIG and Holocene records for pre-defined small regions with high data density. We then calculate regional volume-weighted δ^{13}C means for larger regions from which we estimate the global LIG-Holocene anomaly.

3.1 Regional reconstruction of δ^{13}C

155 We define regions with high densities of cores to reconstruct regional mean δ^{13}C (Fig. 2). These regions need to be small enough to assume reasonably small spatial variability in the δ^{13}C signal and yet still have enough data to establish a reliable statistical difference between the two time periods.

Based on these requirements, four regions are selected: the northeast Atlantic, the equatorial Atlantic, a region off the Namibian Coast (southeast Atlantic), and a region around the Galapagos Islands (eastern equatorial Pacific). The boundaries
160 of each region are defined in Table 1, with values of records deeper than 2,500 m represented in the box plots of Fig. 2c. The statistical characteristics shown in all of the box plots are consistently lower at the LIG compared to the Holocene ranging from 0.1 to 0.3 ‰ lower, which suggests that independent of regional differences, the LIG exhibits lower δ^{13}C values than the Holocene (Fig. 2). However, these box plots include all the data from 130–118 ka BP and 8–2 ka BP, and might therefore capture more than the mean LIG and Holocene states, i.e. they might include parts of the deglaciations or the beginning of the
165 glacial inception for the LIG.

Most δ^{13}C time series display a significant increase in benthic δ^{13}C between 130 and 127 ka BP (Fig. 3). Given the uncertainties in the age models, this increase could be associated with the penultimate deglaciation (Oliver et al., 2010; Menviel et al., 2019). To avoid the relatively low δ^{13}C values which could be associated with the penultimate deglaciation and glacial inception, we focus our analysis on the period 125–120 ka BP (Fig. 3a). We round the data to the nearest 1 ka, find an average
170 per 1 ka, and refer to this as a time slice. We consider qualitatively the influence of changes in the average depth in which the proxies were recorded, as indicated by the direction of the black triangles in Fig. 3. To make a meaningful comparison with the Holocene, we also restrict the Holocene data to a relatively stable δ^{13}C period, spanning from 7 to 4 ka BP for the Holocene–the mid-Holocene. The number of data points per 1 ka time slice deteriorates on either side of these two periods.

The average δ^{13}C anomaly between the LIG and mid-Holocene stable periods as defined above is consistent across the
175 different regions despite their geographic separation, suggesting a significantly lower δ^{13}C during the LIG than the mid-
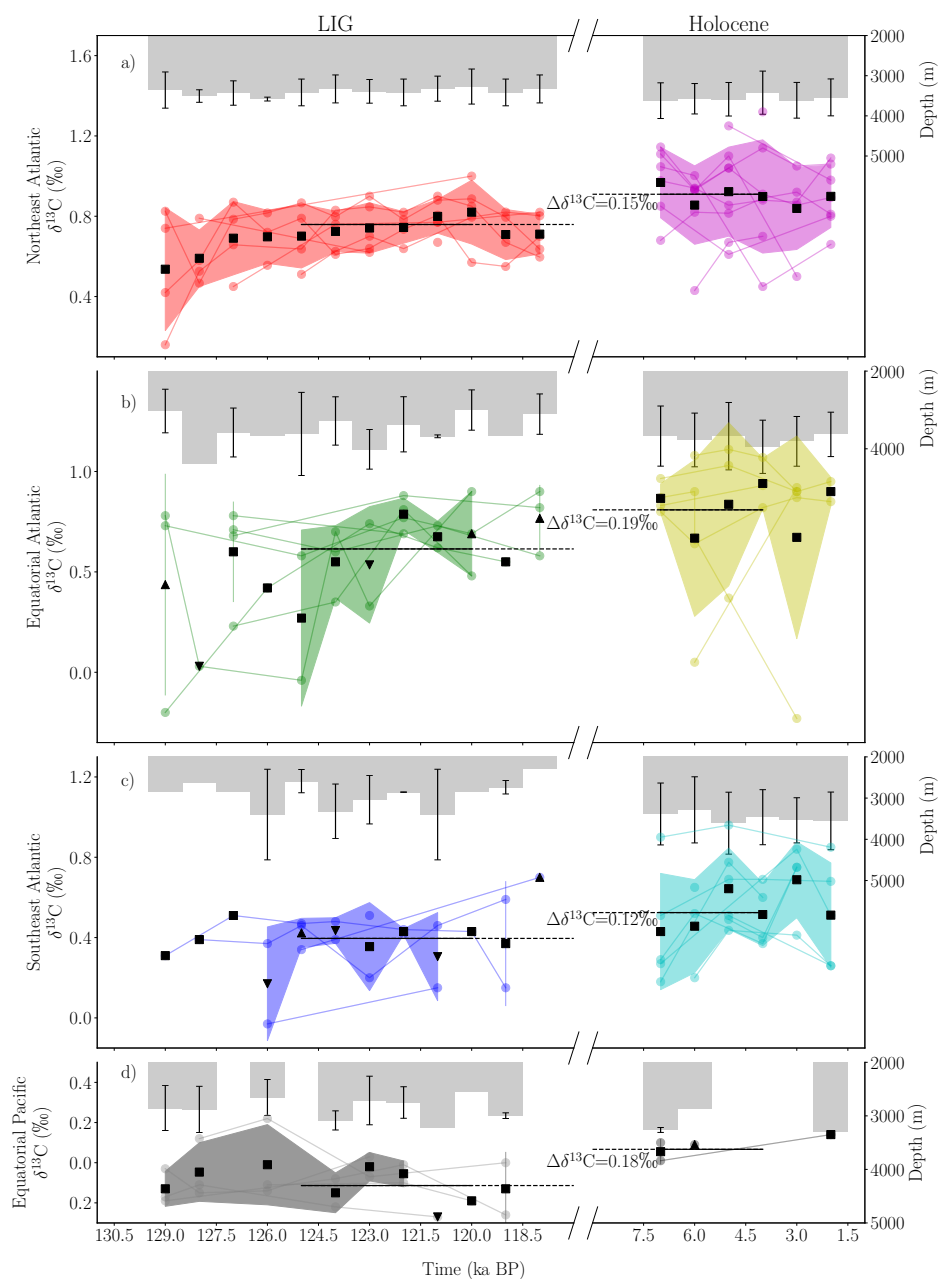
Figure 3. Benthic foraminifera δ^{13}C (left y-axis, ‰) during the LIG (left) and Holocene (right) for four defined regions; northeast Atlantic (a), equatorial Atlantic (b), southeast Atlantic (c), and eastern equatorial Pacific (d). Data is presented in discrete time slices spanning 1 ka, only cores deeper than 2,500 m are shown. Circular, coloured points connected by lines show each average δ^{13}C value per core per time slice. Black symbols represent δ^{13}C averages per slice. Each slice has a corresponding averaged depth (right y-axis, m), with 1 standard deviation on either side shown in the bars. Slices with an average depth within ±300 m of the mean core depth of all slices are represented with a square point. Slices with an average depth shallower than the 300 m less than the mean are shown with an upward triangle, and deeper than 300 m more than the mean are shown with a downward triangle. Shading shows 1 standard deviation on either side of the mean for slices where more than 1 point exists.

Table 2. Regional breakdown of δ^{13}C data during the mid-Holocene (7–4 ka BP) and LIG (125–120 ka BP) averaged across the 1 ka time slices. For each region: the average number of data points (labelled as 'Points') and cores per time slice (labelled as 'Cores'), the average standard deviation of δ^{13}C per time slices (‰), the mean depth (m) across time slices, and the standard deviation of depth (m) between time slices (σ_{depth}). NEA: northeast Atlantic, NWA: northwest Atlantic, SA: south Atlantic, SEA: southeast Atlantic, SWA: southwest Atlantic, I: Indian, NP: north Pacific, SP: south Pacific.

Area	Holocene						LIG					
	δ^{13}C (‰)	Points	Cores	$\sigma_{\delta^{13}C}$ (‰)	Mean depth (m)	σ_{depth} (m)	δ^{13}C (‰)	Points	Cores	$\sigma_{\delta^{13}C}$ (‰)	Mean depth (m)	σ_{depth} (m)
NEA	0.94	72.5	38.5	0.20	2851	33	0.76	26.0	11.8	0.21	2791	15
NWA	0.81	28.5	14.0	0.24	3667	29	0.66	38.5	7.3	0.23	3723	38
SA	0.04	6.0	2.5	0.15	4031	0	-0.16	1.8	1.0	0.06	4616	0
SEA	0.63	10.5	9.5	0.25	3128	122	0.54	6.0	6.0	0.23	3203	24
SWA	0.92	6.0	4.5	0.42	2703	36	0.48	1.5	1.5	0.21	3584	156
I	0.17	6.0	4.5	0.24	2409	100	0.04	3.0	2.8	0.21	2383	0
NP	0.05	12.0	7.0	0.22	2055	103	-0.09	5.0	3.5	0.27	2833	50
SP	0.47	12.5	4.0	0.26	2264	19	0.14	1.5	1.5	0.20	2593	0

Holocene, with differences ranging from 0.13 ‰ in the south-east Atlantic to 0.19 ‰ in the equatorial Atlantic (Table 1). The statistical significance between the two time periods is established using a two-tailed t-test on data that has one value per core and spans the entire time slices (125–120 ka BP and 7–4 ka BP). The t-test shows that there is a statistically significant difference everywhere except in the southeast Atlantic, with confidence intervals varying from 0.14 in the Equatorial Atlantic to 0.06 in the Equatorial Pacific. When using a single tail t-test instead, the difference becomes significant in the southeast Atlantic, giving a new p-value of 0.002. Figure 3 suggests that depth variations between time slices likely explain the variability in this region, making it difficult to establish a difference between the two time periods. However, the mean depth in each region between the LIG and the mid-Holocene are similar (with a maximum difference of 135 m).

Within this stable period during the LIG, a small δ^{13}C increase can be observed in the northeast Atlantic between 125 and 120 ka BP (Fig. 3a). Over that period, a linear regression fitted to the mean of the points suggests an increase in δ^{13}C of 0.02 ‰ ka^{-1}, with a p-value of 0.001 and an R^2 of 0.93, suggesting that while the trend is small, it is statistically significant.

3.2 Volume-weighted regional δ^{13}C

The second approach we use to further constrain the LIG-Holocene δ^{13}C anomaly is to estimate the volume-weighted regional δ^{13}C. We define our regional boundaries based on the regions described in Peterson et al. (2014), however we only include the regions where there is enough data to justify an analysis. For all the data in each of these regions, we calculate a mean value by taking the direct averages of all data below 1,000 m depth. We divide the ocean basins into eight regions (Table 2, shown in Fig. A1 (Peterson et al., 2014)) and calculate the volume-weighted averages δ^{13}C for each of these regions. Since the Atlantic and Pacific Oceans have more data than the Indian Ocean, there is greater confidence in the δ^{13}C estimates for these regions. These regional averages are then used to calculate a global volume-weighted δ^{13}C.

Results for the Atlantic and Pacific Oceans are given in Fig. 4, and show a mean LIG-Holocene anomaly of -0.22 ‰ and -0.24 ‰ respectively, slightly higher than the range of estimates for the four regions selected in Sect. 3.1. The slightly higher offset estimated in the Atlantic compared to our previous regional analysis (Sect. 3.1) could be due to the δ^{13}C records in cores

located in the southwest Atlantic, which were not included in our regional analysis. There are only 4 cores available in this
region during the Holocene, and 1 during the LIG. The estimated LIG-Holocene anomaly is relatively high at -0.4 ‰. However,
200 the relatively large LIG to Holocene anomaly estimate of -0.4 ‰ could be due to the deeper location of the LIG core compared
to the mean of the Holocene cores (881 m, Table 2). There is less confidence in the estimate of the Pacific volume-weighted
mean since the proxy data is sparse, and the majority are from the eastern equatorial Pacific (4 LIG, 11 Holocene) as shown in
Fig. 2.

Similar to the trend highlighted in the northeast Atlantic (Fig. 3a), there is a small positive trend in the average Atlantic
205 δ^{13}C from 125 ka BP, reaching a maximum value at 121 ka BP (Fig. 4). The average core depth over this time period does
not suggest that a change in the mean depth could explain this variation. Fitting a linear regression over this period indicates
an increase in δ^{13}C of 0.03 ‰ ka^{-1} in the Atlantic, with a p-value of 0.03 and an R^2 of 0.72, similar to the trend seen in
the northeast Atlantic (Fig. 3a). This $\sim$0.15 ‰ Atlantic Ocean δ^{13}C increase is also concurrent with the $\sim$0.3 ‰ atmospheric
δ^{13}CO$_2$ increase. For the Pacific, there is a $\sim$0.18 ‰ increase in δ^{13}C between 7 and 5 ka BP, which could be associated with
210 the early Holocene terrestrial regrowth (Menviel and Joos, 2012).

For the Indian Ocean, we only include two cores, as these are the only ones spanning both the LIG and mid-Holocene. An
LIG anomaly of -0.13 ‰ in the Indian Ocean compared to the mid-Holocene is therefore associated with higher uncertainties.
The whole ocean mean LIG δ^{13}C anomaly is -0.21 ‰, but it is associated with higher uncertainties than each region anomaly.

Both the regional analysis of our new database and our volume-weighted estimate indicate that the global mean δ^{13}C was
215 about 0.2 ‰ lower during the LIG than during the mid-Holocene. There are three possible explanations for this difference.
Firstly, an AMOC change might influence the global estimate due to overrepresentation of the Atlantic Ocean in the data.
Since in total only 22 points originate from the Pacific and Indian basins compared to 69 in the Atlantic during the LIG, and
a change in AMOC would significantly impact Atlantic benthic δ^{13}C (Menviel et al., 2015), an assessment of possible mean
LIG AMOC change would provide additional confidence in a global mean ocean δ^{13}C change. Secondly, the global estimate
220 might be influenced by lower LIG than mid-Holocene stores of organic carbon in either the land biosphere or dissolved organic
matter. Thirdly, changes in sedimentary and lithospheric carbon both in terms of quantity and mean δ^{13}C value can impact the
global mean δ^{13}C (Jeltsch-Thömmes and Joos, 2020; Schneider et al., 2013). These three possibilities are explored below.

3.3 Reconstruction of the LIG Atlantic Meridional Overturning Circulation

In this section, we analyse the spatial δ^{13}C distribution in the Atlantic Ocean to assess potential changes in the penetration
225 depth and southward expansion of NADW during the LIG, defined here as 125–120 ka BP, with respect to the mid-Holocene.
A change in NADW might influence our estimate of the mean δ^{13}C, given that most of the available data is localised in the
Atlantic Ocean.

We use simple statistical regression models to reconstruct NADW and AABW separately with a quadratic-with-depth and
linear-with-latitude equation following the method of Bengtson et al. (2019). For consistency, the regression algorithm only
230 includes records from cores that span both the LIG and mid-Holocene and uses a weighted least squares approach, where the
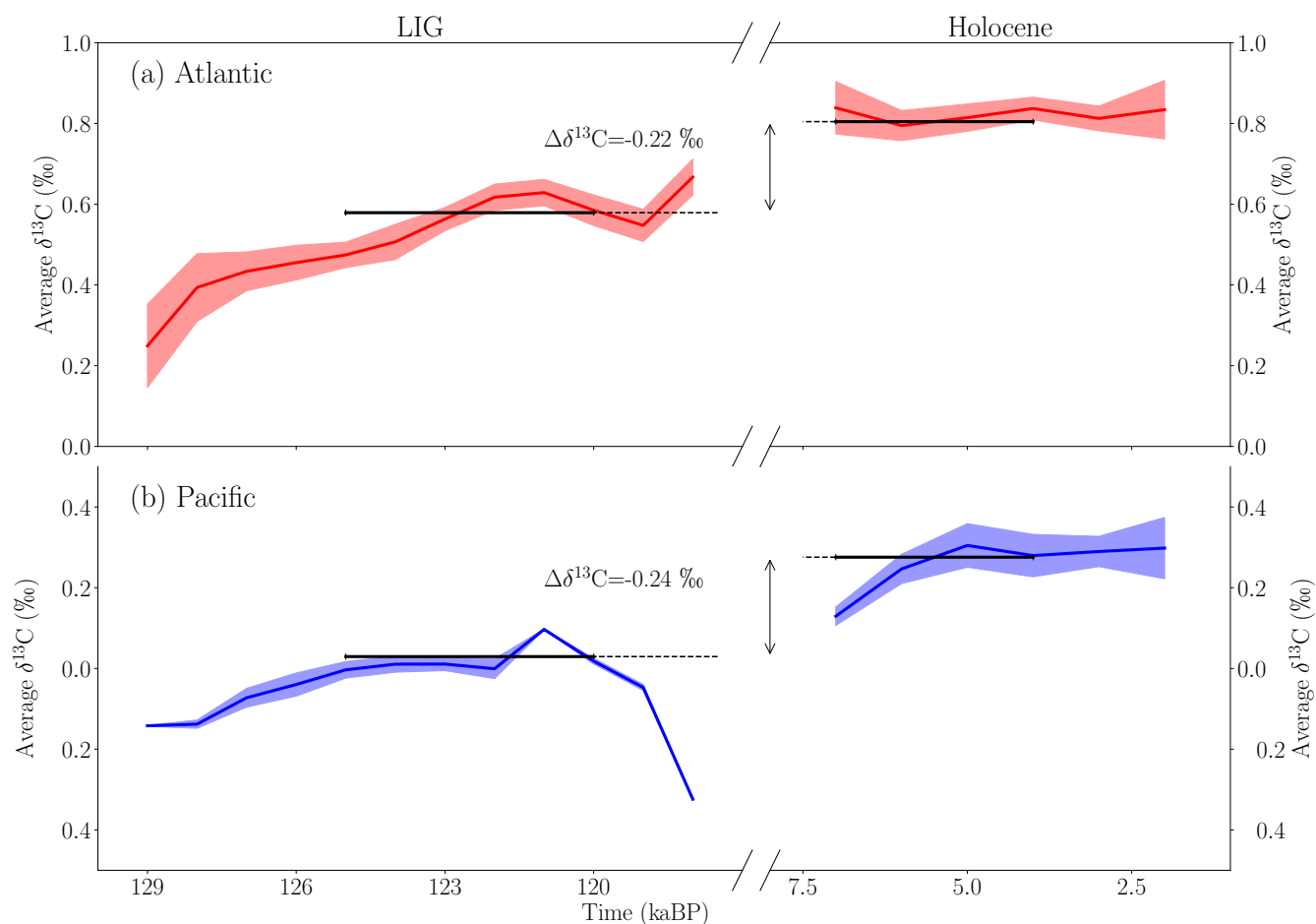
Figure 4. Comparison of volume-weighted δ^{13}C for the Atlantic (red) and Pacific (blue) for the LIG and mid-Holocene, calculated using the regions from Peterson et al. (2014). Solid coloured lines indicate the mean volume-weighted δ^{13}C, and the shading indicates the volume-weighted sum of square deviations from the mean. The horizontal bars indicate the mean of the stable period determined from the regional analysis as defined in Sect. 3.1 (LIG: 125–120 ka BP, mid-Holocene: 7–4 ka BP), with the $\Delta\delta^{13}$C indicating the mean anomaly between these two average.

weighting equals the number of samples per core. The modelled region is defined between 40° S and 60° N as this is the region
where we can expect to find both the NADW and AABW δ^{13}C signals.

The results are shown in Fig. 5. We test the robustness of our statistical model using the jackknifing technique. We systemati-
cally exclude each individual core from the database one at a time, fit the parameters using this modified database, and compare
235   the model prediction against the core which was excluded. This produces small variations in the average mean response of the
statistical models (the standard deviations were 0.04 ‰ and 0.03 ‰ for the LIG and mid-Holocene, respectively).

We calculate end-member values based on proxies located near the water mass sources. These are taken as 0.79 ‰ and 1.02
‰ for NADW for the LIG and mid-Holocene, respectively, and -0.09 ‰ and 0.22 ‰ for AABW for the LIG and mid-Holocene,
respectively. The end-member values are calculated as the average of cores shallower than 3,000 m but deeper than 1,000 m
240   and located between 50° N and 70° N for NADW. The NADW end-member cores have an average depth of 2043 m and a
standard deviation of 478 m. For the AABW end-member, the only eligible core is ODP1089, which is at ∼41° S and 4621 m.
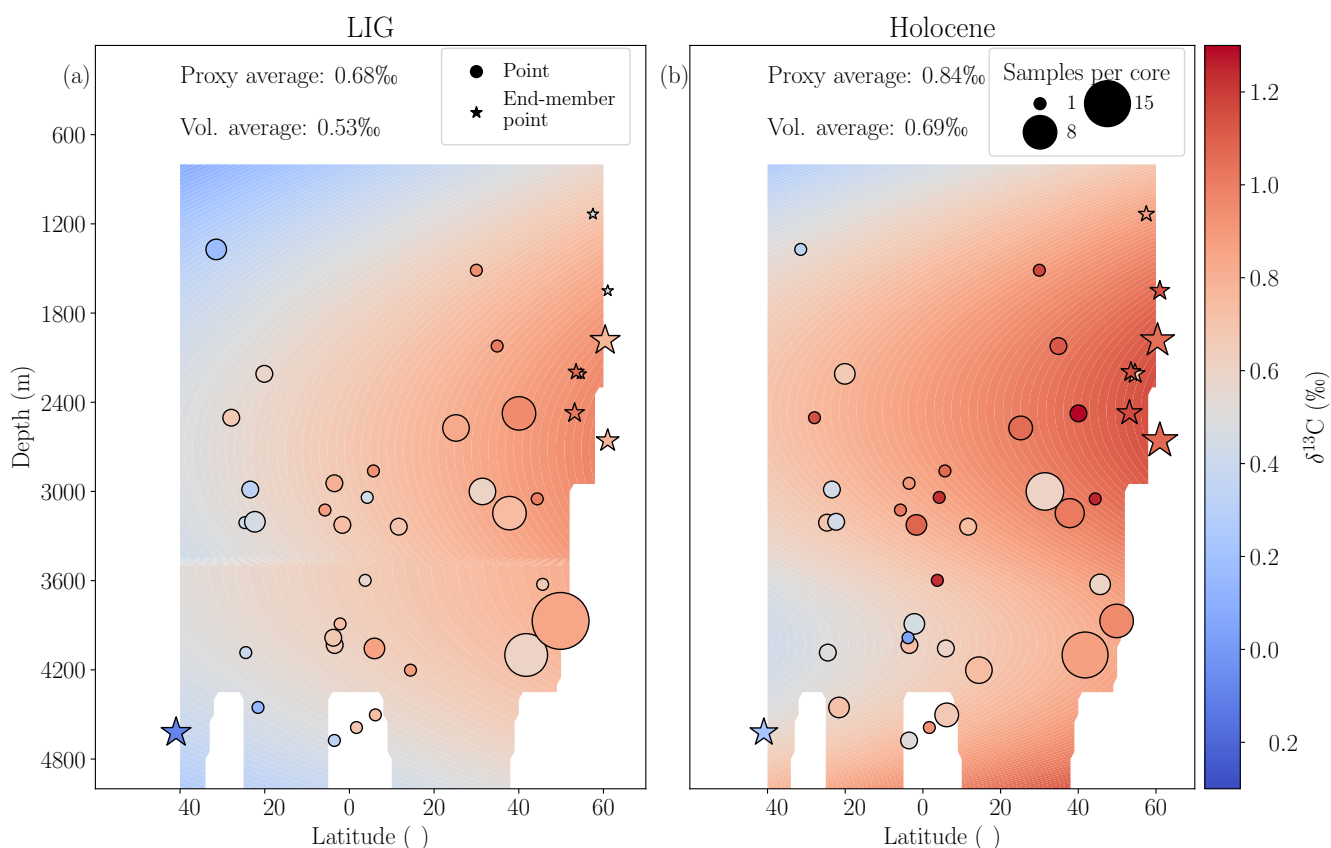
Figure 5. Reconstructed Atlantic δ^{13}C (‰) meridional section during the LIG and mid-Holocene. The circular points represent the proxy
data, showing the average δ^{13}C with colour and the number of points per core with size. The stars represent the proxy data which make up
the end-members. Background shading shows the reconstructed δ^{13}C.

The mean volume-weighted δ^{13}C for the Atlantic Ocean between 40° S and 60° N based on this interpolation is 0.53 ‰ for the LIG and 0.69 ‰ for the mid-Holocene (Fig. 5). This suggests a 0.16 ‰ lower Atlantic δ^{13}C at the LIG than the mid-Holocene. Our statistical reconstruction points to a very similar NADW depth (∼2,600 m) for both time periods (Fig. 5). The

245 NADW depth is defined here as the depth of maximum δ^{13}C in the North Atlantic.

We also investigate the meridional gradient in δ^{13}C in the Atlantic Ocean to determine whether the NADW southward penetration, transport and remineralisation rates were significantly different during the LIG compared to the mid-Holocene. We only consider cores that are located between depths of 1,000 and 3,000 m in order to stay within the main pathway of NADW (Fig. 6a). Though there is significant scatter, in accordance with our previous findings, a moving average through the

250 Holocene and the LIG data shows that LIG δ^{13}C is typically lower than the mid-Holocene counterparts. However, the slopes of the meridional δ^{13}C statistical model gradients are not very different for the LIG (0.0050 ‰ °latitude^{-1}) and the mid-Holocene (0.0045 ‰ °latitude^{-1}) (Fig. 6a), suggesting a similar southward penetration of NADW.
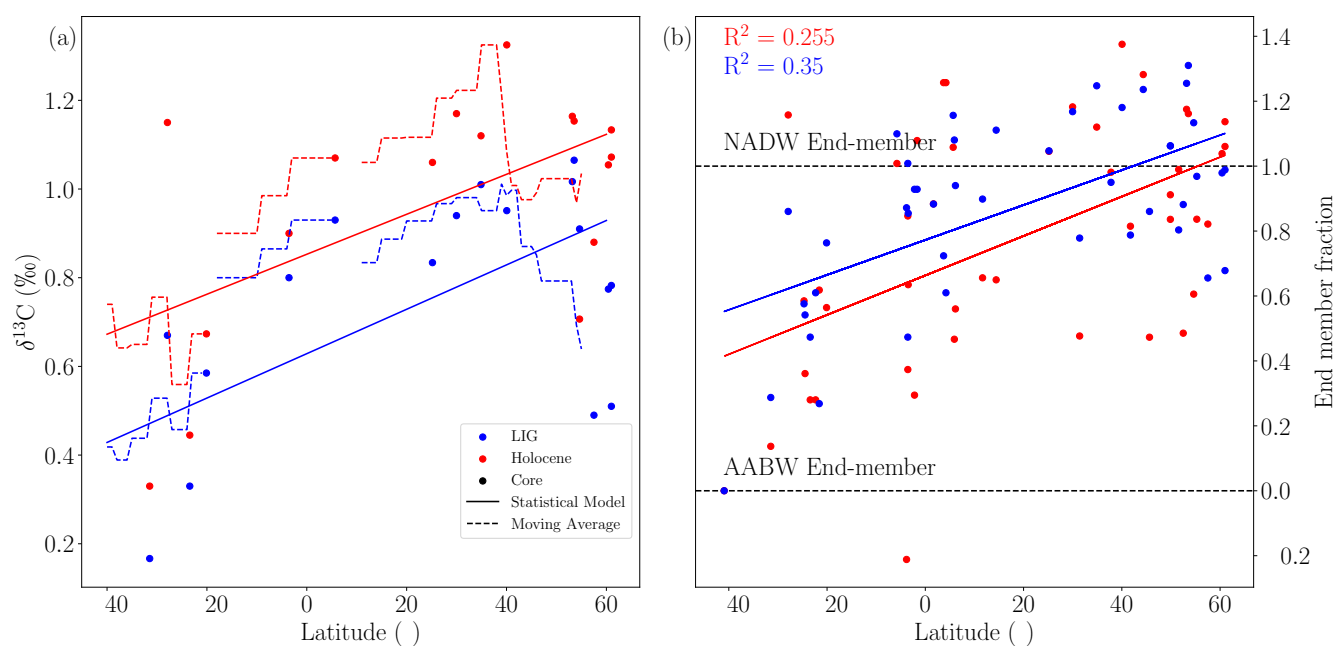
Figure 6. The meridional gradient of the Atlantic Ocean benthic δ^{13}C (‰). a) Mid-Holocene (red) and LIG (blue) $\delta^{13}C$ for each core (points) between 1,000 m and 3,000 m. Dotted lines are the moving averages of the cores. Solid lines indicate the results of our statistical model at 2,000 m. b) Average δ^{13}C for each record deeper than 1,000 m as a proportion of the end-members. A value of one indicates the NADW end-member and a value of zero the AABW end-member. Solid lines show the linear regressions of the records.

Using δ^{13}C of the end-members for NADW and AABW, we use a simple binary mixing model for all cores deeper than 1,000 m to estimate changes in NADW penetration (Fig. 6b). The LIG and mid-Holocene δ^{13}C slopes in the Atlantic are

255 similar, indicating similar southward penetration of NADW during both time periods. This suggests that the differences in

δ^{13}C between the two time periods is most likely due to change in end-member values, while the mean Atlantic oceanic circulation was likely similar.

Based on our analysis, there appears to be no significant difference in the mean time-averaged AMOC between the LIG and the mid-Holocene. Negative LIG-Holocene anomalies are found for each of the smaller regions selected (northeast Atlantic, equatorial Atlantic, southeast Atlantic, and eastern equatorial Pacific), with statistical significance seen in all regions except the southeast Atlantic, where depth variations between time slices likely explain the increased variability in this region. Additionally, our volume-weighted mean δ^{13}C estimates display similar anomalies in the Atlantic and Pacific Oceans (-0.22 ‰ and -0.24 ‰ respectively).

4 Discussion

One of the goals of our study is to assess the mean change in oceanic δ^{13}C between the LIG and the Holocene. Given the uncertainties in the chronologies and to avoid taking into account data that would pertain to deglaciations, we chose the periods 125 to 120 ka BP for the LIG and 7 to 4 ka BP for the mid-Holocene. Using a similar geographical distribution of data points for both periods, we find that the oceanic δ^{13}C was ∼0.2 ‰ lower during the LIG than the mid-Holocene.

Our analysis of the δ^{13}C signal suggests consistent LIG-Holocene δ^{13}C anomalies in different regions of the Atlantic basins, as well as in the Pacific and Indian Oceans, even if there are significant uncertainties with the later due to fewer available records. The δ^{13}C distribution in the Atlantic Ocean suggests that there was no significant mean change in the southward penetration or depth of NADW during the LIG compared to the mid-Holocene. However, because of the relatively large time slices that were used in our analysis (1 ka) and with a typical age model uncertainty of ±2 ka, our analysis suggests that there is no difference in the mean oceanic circulation between the periods 125–120 ka BP and 7–4 ka BP without being able to resolve potential centennial-scale oceanic circulation changes (e.g. Tzedakis et al., 2018).

The overall 0.2 ‰ lower oceanic δ^{13}C could potentially be due to a change in end-member values (Fig. 6). As fractionation during air-sea gas exchange is temperature dependent, globally higher SSTs at the LIG could lead to a lower oceanic δ^{13}C. However, this would also lead to a higher atmospheric $\delta^{13}CO_2$ at the LIG, which is inconsistent with Antarctic ice core measurements (Schneider et al., 2013). Nutrient utilisation decrease in the North Atlantic could also decrease surface ocean δ^{13}C and thus the δ^{13}C end-members. However, because the vast amount of organic carbon is remineralised and therefore remains as DIC (Sarmiento et al., 2002), nutrient utilisation impact on the end-members should not have influenced the average oceanic mean δ^{13}C, unlike the process of air-sea gas exchange. Currently, there is still a lack of constraints on nutrient utilisation in these end-member regions during the LIG compared to the Holocene.

Since both the atmospheric and oceanic δ^{13}C were lower at the LIG than during the Holocene, this could indicate a significant release of low δ^{13}C terrestrial carbon into the system. While changes in the terrestrial biosphere are not well constrained during the LIG, the proxies do indicate that there was possibly a greener Sahara (Larrasoaña et al., 2013) and a greater forest coverage at high latitudes (CAPE, 2006; Tarasov et al., 2005; Muhs et al., 2001; de Vernal and Hillaire-Marcel, 2008; Govin et al., 2015), which should have increased the carbon stored in the terrestrial vegetation. This does not account for other factors though, such

as the intensity of fires, which can have a significant impact on the terrestrial carbon storage (Bowman et al., 2009). A lower
terrestrial carbon reservoir could also be explained by a decrease in soil carbon, including changes in carbon stored in peatlands
and permafrost. While, to our knowledge, no comprehensive proxy-based reconstruction of soil carbon during the LIG exists,
one modelling study found that the increase in carbon storage during the LIG was almost offset by an increase in heterotrophic
respiration caused by higher temperatures at high latitudes (Schurgers et al., 2006), which gives credence to a lower soil carbon
reservoir between the LIG and the mid-Holocene.

Furthermore, it is estimated that ∼550 Gt C are stored in high northern latitude peats today (Yu et al., 2010), with a mean
δ^{13}C value of ∼-28 ‰ (Dioumaeva et al., 2002; Novák et al., 1999). Any variation in peat accumulation rates could therefore
significantly impact the total terrestrial carbon storage. Though it is associated with large uncertainties, a modelling study
indicated higher accumulation of carbon in peat during the LIG than during the Holocene (Kleinen et al., 2012). Recent
estimates suggest that ∼1,500 Gt C are stored in permafrost, with about 1,000 Gt C in the active layer (Schuur et al., 2015).
Even though quantitative estimates are lacking, there is some evidence in Siberia and Alaska for thawing permafrost during the
LIG due to warmer conditions, potentially leading to a carbon release (e.g. Reyes et al., 2010; Stapel et al., 2018). Currently,
both our understanding of the carbon stored in permafrost in the past and the potential evolution of permafrost in the future is
limited (Turetsky et al., 2020). Further research to constrain this aspect of the climate system is needed.

While there is possibility of carbon stored in vegetation and soils contributing to the δ^{13}C anomaly that we have observed, we
are unable to verify this through the use of a mass balance, since the atmosphere–biosphere–ocean system cannot be assumed
to be closed (Jeltsch-Thömmes and Joos, 2020).

At the LIG, both atmospheric $\delta^{13}CO_2$ and oceanic δ^{13}C were lower than during the mid-Holocene, with atmosphere and
ocean anomalies being 0.3 ‰ (Schneider et al., 2013) and 0.2 ‰ respectively. Such multi-millenial differences in the isotopic
signal of both the atmosphere and ocean were most likely due to a long-term imbalance between weathering and sedimentation
of carbon (Jeltsch-Thömmes and Joos, 2020).

5 Conclusions

We present a new compilation of benthic δ^{13}C from 130 to 115 ka BP covering the LIG. Over this time period, benthic δ^{13}C
generally display a maximum value at ∼121 ka BP (±2 ka), in phase with the maximum atmospheric $\delta^{13}CO_2$ (LIG value
of -6.5 ‰ at ∼120 ka BP). As there are significant chronological uncertainties associated with LIG records, we identify a
relatively stable period ranging between 125 and 120 ka BP. We compare this LIG benthic δ^{13}C data to a similar database
covering the mid-Holocene (7-4 ka BP). We find that during these specific time periods, LIG oceanic δ^{13}C was about 0.2 ‰
lower than during the mid-Holocene. This anomaly is consistent across different regions in the Atlantic Ocean. Even though
there are less records available, benthic δ^{13}C data from the Pacific Ocean also support an anomaly of about 0.2 ‰.

An analysis of δ^{13}C gradients across the Atlantic Ocean suggests that there were no significant changes in mean, long-
term ocean circulation across the two intervals. While reduced high northern latitude peat and permafrost caused by higher
temperatures at the LIG than during the mid-Holocene (Otto-Bliesner et al., 2020) could also lead to a lower atmospheric and

oceanic δ^{13}C, the most likely explanation for the lower LIG oceanic δ^{13}C is a long term imbalance in the weathering and burial of carbon. Additional studies are required to further constrain the LIG carbon balance.

Appendix A: Regional Boundaries
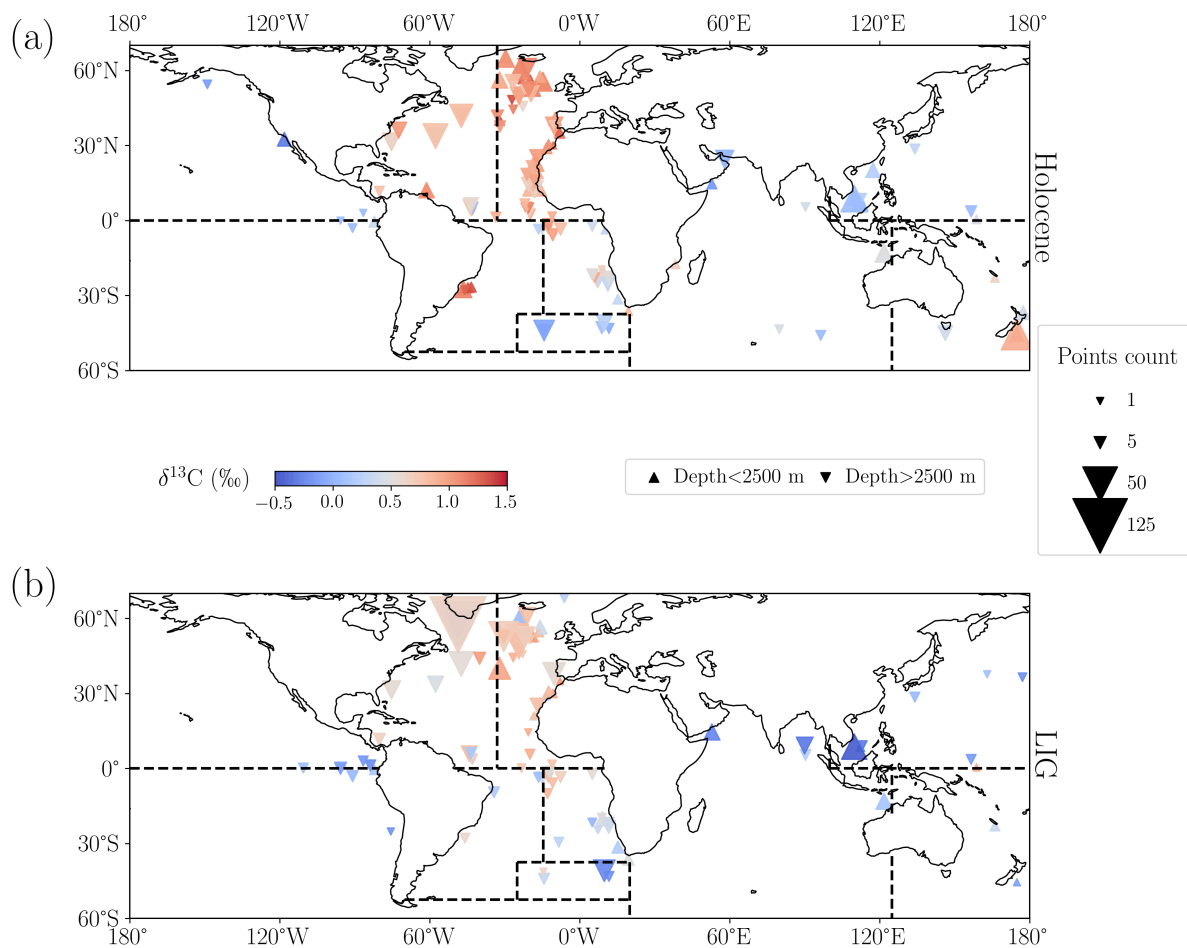
Figure A1. Global distribution of benthic foraminifera δ^{13}C (‰) during the Holocene (a) and LIG (b) showing the regional boundaries used to calculate the global volume-weighted mean δ^{13}C. Dotted black lines indicate the regional boundaries. Symbol size indicates the number of values per core, colour indicates average δ^{13}C, and the triangle direction indicates the proxy depth (upward-pointing triangle: shallower than 2,500 m, downward-pointing triangle: deeper than 2,500 m).

325   *Author contributions.* SAB, LCM, and KJM designed the research. CDP and LEL provided significant portions of the δ^{13}C data. SAB, LCM, KJM, and LM analysed the data and developed the methodology. FJ assisted in the interpretation of the results. SAB prepared the manuscript with contributions from all co-authors.

Competing interests. The authors declare that they have no conflict of interest.

Acknowledgements. Shannon Bengtson acknowledges funding from the Australian Government Research Training Program Scholarship.
330 Laurie Menviel and Katrin Meissner acknowledge funding from the Australian Research Council grants FT180100606 (to Laurie Menviel) and DP180100048 (to Katrin Meissner and Laurie Menviel). Computational resources were provided by the NCI National Facility at the Australian National University, through awards under the Merit Allocation Scheme, the Intersect allocation scheme, and the UNSW HPC at NCI Scheme. Fortunat Joos acknowledges funding from the Swiss National Science Foundation (#200020_172476).

References

335   Anderson, R. S., Jiménez-Moreno, G., Ager, T., and Porinchu, D. F.: High-Elevation Paleoenvironmental Change during MIS 6–4 in the Central Rockies of Colorado as Determined from Pollen Analysis, Quaternary Research, 82, 542–552, https://doi.org/10.1016/j.yqres.2014.03.005, 2014.

Axford, Y., Briner, J., R. Francis, D., H. Miller, G., R. Walker, I., and Wolfe, A.: Chironomids Record Terrestrial Temperature Changes throughout Arctic Interglacials of the Past 200,000 Yr, Geological Society of America Bulletin, 123, 1275–1287,
340   https://doi.org/10.1130/B30329.1, 2011.

Bakker, P., Stone, E. J., Charbit, S., Gröger, M., Krebs-Kanzow, U., Ritz, S. P., Varma, V., Khon, V., Lunt, D. J., Mikolajewicz, U., Prange, M., Renssen, H., Schneider, B., and Schulz, M.: Last Interglacial Temperature Evolution – a Model Inter-Comparison, Climate of the Past, 9, 605–619, https://doi.org/https://doi.org/10.5194/cp-9-605-2013, 2013.

Basu, S., Agrawal, S., Sanyal, P., Mahato, P., Kumar, S., and Sarkar, A.: Carbon Isotopic Ratios of Modern C3–C4 Plants from the
345   Gangetic Plain, India and Its Implications to Paleovegetational Reconstruction, Palaeogeography Palaeoclimatology Palaeoecology, 440, https://doi.org/10.1016/j.palaeo.2015.08.012, 2015.

Belanger, P. E., Curry, W. B., and Matthews, R. K.: Core-Top Evaluation of Benthic Foraminiferal Isotopic Ratios for Paleo-Oceanographic Interpretations, Palaeogeography, Palaeoclimatology, Palaeoecology, 33, 205–220, https://doi.org/10.1016/0031-0182(81)90039-0, 1981.

Bengtson, S. A., Meissner, K. J., Menviel, L., A. Sisson, S., and Wilkin, J.: Evaluating the Extent of North Atlantic Deep Water and the Mean
350   Atlantic δ^{13}C from Statistical Reconstructions, Paleoceanography and Paleoclimatology, https://doi.org/10.1029/2019PA003589, 2019.

Bereiter, B., Eggleston, S., Schmitt, J., Nehrbass-Ahles, C., Stocker, T. F., Fischer, H., Kipfstuhl, S., and Chappellaz, J.: Revision of the EPICA Dome C CO_2 Record from 800 to 600 kyr before Present, Geophysical Research Letters, 42, 542–549, https://doi.org/10.1002/2014GL061957, 2015.

Böhm, E., Lippold, J., Gutjahr, M., Frank, M., Blaser, P., Antz, B., Fohlmeister, J., Frank, N., Andersen, M. B., and Deininger, M.: Strong and
355   Deep Atlantic Meridional Overturning Circulation during the Last Glacial Cycle, Nature, 517, 73–76, https://doi.org/10.1038/nature14059, 2015.

Bowman, D. M. J. S., Balch, J. K., Artaxo, P., Bond, W. J., Carlson, J. M., Cochrane, M. A., D'Antonio, C. M., DeFries, R. S., Doyle, J. C., Harrison, S. P., Johnston, F. H., Keeley, J. E., Krawchuk, M. A., Kull, C. A., Marston, J. B., Moritz, M. A., Prentice, I. C., Roos, C. I., Scott, A. C., Swetnam, T. W., van der Werf, G. R., and Pyne, S. J.: Fire in the Earth System, Science, 324, 481–484,
360   https://doi.org/10.1126/science.1163886, 2009.

Brewer, S., Guiot, J., Sánchez-Goñi, M. F., and Klotz, S.: The Climate in Europe during the Eemian: A Multi-Method Approach Using Pollen Data, Quaternary Science Reviews, 27, 2303–2315, https://doi.org/10.1016/j.quascirev.2008.08.029, 2008.

CAPE: Last Interglacial Arctic Warmth Confirms Polar Amplification of Climate Change, Quaternary Science Reviews, 25, 1383–1400, https://doi.org/10.1016/j.quascirev.2006.01.033, 2006.

365   Capron, E., Govin, A., Feng, R., Otto-Bliesner, B. L., and Wolff, E. W.: Critical Evaluation of Climate Syntheses to Benchmark CMIP6/PMIP4 127 ka Last Interglacial Simulations in the High-Latitude Regions, Quaternary Science Reviews, 168, 137–150, https://doi.org/10.1016/j.quascirev.2017.04.019, 2017.

Cernusak, L. A., Ubierna, N., Winter, K., Holtum, J. A. M., Marshall, J. D., and Farquhar, G. D.: Environmental and Physiological Determinants of Carbon Isotope Discrimination in Terrestrial Plants, New Phytologist, 200, 950–965, https://doi.org/10.1111/nph.12423,
370   2013.

Curry, W. B. and Oppo, D. W.: Glacial Water Mass Geometry and the Distribution of $\delta^{13}C$ of ΣCO_2 in the Western Atlantic Ocean, Paleoceanography, 20, https://doi.org/10.1029/2004PA001021, 2005.

de Vernal, A. and Hillaire-Marcel, C.: Natural Variability of Greenland Climate, Vegetation, and Ice Volume During the Past Million Years, Science, 320, 1622–1625, https://doi.org/10.1126/science.1153929, 2008.

375 Diefendorf, A. F. and Freimuth, E. J.: Extracting the Most from Terrestrial Plant-Derived n-Alkyl Lipids and Their Carbon Isotopes from the Sedimentary Record: A Review, Organic Geochemistry, 103, 1–21, https://doi.org/10.1016/j.orggeochem.2016.10.016, 2017.

Diefendorf, A. F., Mueller, K. E., Wing, S. L., Koch, P. L., and Freeman, K. H.: Global Patterns in Leaf ^{13}C Discrimination and Implications for Studies of Past and Future Climate, Proceedings of the National Academy of Sciences, 107, 5738–5743, https://doi.org/10.1073/pnas.0910513107, 2010.

380 Dioumaeva, I., Trumbore, S., Schuur, E. A. G., Goulden, M. L., Litvak, M., and Hirsch, A. I.: Decomposition of Peat from Upland Boreal Forest: Temperature Dependence and Sources of Respired Carbon, Journal of Geophysical Research: Atmospheres, 107, 8222, https://doi.org/10.1029/2001JD000848, 2002.

Drake, N. A., Blench, R. M., Armitage, S. J., Bristow, C. S., and White, K. H.: Ancient Watercourses and Biogeography of the Sahara Explain the Peopling of the Desert, Proceedings of the National Academy of Sciences, 108, 458–462, https://doi.org/10.1073/pnas.1012231108, 385 2011.

Duplessy, J.-C., Shackleton, N. J., Matthews, R. K., Prell, W., Ruddiman, W. F., Caralp, M., and Hendy, C. H.: ^{13}C Record of Benthic Foraminifera in the Last Interglacial Ocean: Implications for the Carbon Cycle and the Global Deep Water Circulation, Quaternary Research, 21, 225–243, https://doi.org/10.1016/0033-5894(84)90099-1, 1984.

Dutton, A. and Lambeck, K.: Ice Volume and Sea Level During the Last Interglacial, Science, 337, 216–219, 390 https://doi.org/10.1126/science.1205749, 2012.

Dutton, A., Carlson, A. E., Long, A. J., Milne, G. A., Clark, P. U., DeConto, R., Horton, B. P., Rahmstorf, S., and Raymo, M. E.: Sea-Level Rise Due to Polar Ice-Sheet Mass Loss during Past Warm Periods, Science, 349, aaa4019, https://doi.org/10.1126/science.aaa4019, 2015.

Eggleston, S., Schmitt, J., Bereiter, B., Schneider, R., and Fischer, H.: CO_2 Concentration and Stable Isotope Ratios of Three Antarctic Ice Cores Covering the Period from 149.4 - 1.5 kyr before 1950, https://doi.org/10.1594/PANGAEA.859181, 2016a.

395 Eggleston, S., Schmitt, J., Bereiter, B., Schneider, R., and Fischer, H.: Evolution of the Stable Carbon Isotope Composition of Atmospheric CO_2 over the Last Glacial Cycle, Paleoceanography, 31, 2015PA002 874, https://doi.org/10.1002/2015PA002874, 2016b.

Eide, M., Olsen, A., Ninnemann, U. S., and Johannessen, T.: A Global Ocean Climatology of Preindustrial and Modern Ocean $\delta^{13}C$, Global Biogeochemical Cycles, 31, 515–534, https://doi.org/10.1002/2016GB005473, 2017.

Elsig, J., Schmitt, J., Leuenberger, D., Schneider, R., Eyer, M., Leuenberger, M., Joos, F., Fischer, H., and Stocker, T. F.: Carbon Isotopic 400 Record of CO_2 from the Holocene of the Dome C Ice Core, https://doi.org/10.1594/PANGAEA.728699, 2009.

Farquhar, G. D.: On the Nature of Carbon Isotope Discrimination in C4 Species, Functional Plant Biology, 10, 205–226, https://doi.org/10.1071/pp9830205, 1983.

Farquhar, G. D., Ehleringer, J. R., and Hubick, K. T.: Carbon Isotope Discrimination and Photosynthesis, Annual Review of Plant Physiology and Plant Molecular Biology, 40, 503–537, https://doi.org/10.1146/annurev.pp.40.060189.002443, 1989.

405 Flückiger, J., Monnin, E., Stauffer, B., Schwander, J., Stocker, T. F., Chappellaz, J., Raynaud, D., and Barnola, J.-M.: High-Resolution Holocene N_2O Ice Core Record and Its Relationship with CH_4 and CO_2, Global Biogeochemical Cycles, 16, 10–1–10–8, https://doi.org/10.1029/2001GB001417, 2002.

Galaasen, E. V., Ninnemann, U. S., Irvalı, N., Kleiven, H. F., Rosenthal, Y., Kissel, C., and Hodell, D. A.: Stable Isotope Ratios of C. Wueller-storfi from Sediment Core MD03-2664, Bjerknes Centre for Climate Research, https://doi.org/https://doi.org/10.1594/PANGAEA.830079,
410   2014a.

Galaasen, E. V., Ninnemann, U. S., Irvalı, N., Kleiven, H. K. F., Rosenthal, Y., Kissel, C., and Hodell, D. A.: Rapid Reductions in North Atlantic Deep Water During the Peak of the Last Interglacial Period, Science, 343, 1129–1132, https://doi.org/10.1126/science.1248667, 2014b.

Govin, A.: 4) Planktic and Benthic Foraminiferal Stable Isotope Data from Core MD95-2042: Revised Chronology for the Last Interglacial
415   (Period 135-110 Ka), In supplement to: Govin, Aline; Braconnot, Pascale; Capron, Emilie; Cortijo, Elsa; Duplessy, Jean-Claude; Jansen, Eystein; Labeyrie, Laurent D; Landais, Amaelle; Marti, O; Michel, Elisabeth; Mosquet, E; Risebrobakken, Bjørg; Swingedouw, Didier; Waelbroeck, Claire (2012): Persistent influence of ice sheet melting on high northern latitude climate during the early Last Interglacial. Climate of the Past, 8, 483-507, https://doi.org/10.5194/cp-8-483-2012, https://doi.org/10.1594/PANGAEA.777659, 2012.

Govin, A., Braconnot, P., Capron, E., Cortijo, E., Duplessy, J.-C., Jansen, E., Labeyrie, L., Landais, A., Marti, O., Michel, E., Mosquet, E.,
420   Risebrobakken, B., Swingedouw, D., and Waelbroeck, C.: Persistent Influence of Ice Sheet Melting on High Northern Latitude Climate during the Early Last Interglacial, Climate of the Past, 8, 483–507, https://doi.org/https://doi.org/10.5194/cp-8-483-2012, 2012.

Govin, A., Capron, E., Tzedakis, P. C., Verheyden, S., Ghaleb, B., Hillaire-Marcel, C., St-Onge, G., Stoner, J. S., Bassinot, F., Bazin, L., Blunier, T., Combourieu-Nebout, N., El Ouahabi, A., Genty, D., Gersonde, R., Jimenez-Amat, P., Landais, A., Martrat, B., Masson-Delmotte, V., Parrenin, F., Seidenkrantz, M. S., Veres, D., Waelbroeck, C., and Zahn, R.: Sequence of Events from the Onset to the Demise
425   of the Last Interglacial: Evaluating Strengths and Limitations of Chronologies Used in Climatic Archives, Quaternary Science Reviews, 129, 1–36, https://doi.org/10.1016/j.quascirev.2015.09.018, 2015.

Helmens, K. F., Salonen, J. S., Plikk, A., Engels, S., Väliranta, M., Kylander, M., Brendryen, J., and Renssen, H.: Major Cooling Intersecting Peak Eemian Interglacial Warmth in Northern Europe, Quaternary Science Reviews, 122, 293–299, https://doi.org/10.1016/j.quascirev.2015.05.018, 2015.

430   Hodell, D. A., Channell, J. E. T., Curtis, J. H., Romero, O. E., and Röhl, U.: Oxygen and Carbon Isotopes of the Benthic Foraminifer Cibicoides Wuellerstorfi of IODP Site 303-U1308, In supplement to: Hodell, DA et al. (2008): Onset of 'Hudson Strait' Heinrich Events in the eastern North Atlantic at the end of the middle Pleistocene transition (~640 ka)? Paleoceanography, 23(4), PA4218, https://doi.org/10.1029/2008PA001591, https://doi.org/10.1594/PANGAEA.831735, 2008.

Hoffman, J. S., Clark, P. U., Parnell, A. C., and He, F.: Regional and Global Sea-Surface Temperatures during the Last Interglaciation,
435   Science, 355, 276–279, https://doi.org/10.1126/science.aai8464, 2017.

Hoogakker, B. A. A., Rohling, E. J., Palmer, M. R., Tyrrell, T., and Rothwell, R. G.: Underlying Causes for Long-Term Global Ocean $\delta 13C$ Fluctuations over the Last 1.20 Myr, Earth and Planetary Science Letters, 248, 15–29, https://doi.org/10.1016/j.epsl.2006.05.007, 2006.

IPCC: Climate Change 2013: The Physical Science Basis. Contribution of Working Group I to the Fifth Assessment Report of the Inter-governmental Panel on Climate Change, Tech. rep., Cambridge University Press, Cambridge, United Kingdom and New York, NY, USA,
440   2013.

Irvalı, N., Ninnemann, U., Galaasen, E., Rosenthal, Y., Kroon, D., W. Oppo, D., Kleiven, H., Darling, K., and Kissel, C.: Rapid Switches in Subpolar North Atlantic Hydrography and Climate during the Last Interglacial (MIS 5e), Paleoceanography, 27, https://doi.org/10.1029/2011PA002244, 2012.

Jeltsch-Thömmes, A. and Joos, F.: The Response to Pulse-like Perturbations in Atmospheric Carbon and Carbon Isotopes, Climate of the
445   Past Discussions, pp. 1–36, https://doi.org/https://doi.org/10.5194/cp-2019-107, 2020.

Jeltsch-Thömmes, A., Battaglia, G., Cartapanis, O., Jaccard, S. L., and Joos, F.: Low Terrestrial Carbon Storage at the Last Glacial Maximum: Constraints from Multi-Proxy Data, Climate of the Past, 15, 849–879, https://doi.org/z', 2019.

Jeltsch-Thömmes, A. and Joos, F.: Modeling the evolution of pulse-like perturbations in atmospheric carbon and carbon isotopes: the role of weathering–sedimentation imbalances, Climate of the Past, 16, 423–451, https://doi.org/https://doi.org/10.5194/cp-16-423-2020, https://www.clim-past.net/16/423/2020/, 2020.

Jouzel, J. and Masson-Delmotte, V.: EPICA Dome C Ice Core 800KYr Deuterium Data and Temperature Estimates, https://doi.org/10.1594/PANGAEA.683655, 2007.

Kaspar, F., Kühl, N., Cubasch, U., and Litt, T.: A Model-Data Comparison of European Temperatures in the Eemian Interglacial, Geophysical Research Letters, 32, https://doi.org/10.1029/2005GL022456, 2005.

Kawamura, K., Parrenin, F., Lisiecki, L., Uemura, R., Vimeux, F., Severinghaus, J. P., Hutterli, M. A., Nakazawa, T., Aoki, S., Jouzel, J., Raymo, M. E., Matsumoto, K., Nakata, H., Motoyama, H., Fujita, S., Goto-Azuma, K., Fujii, Y., and Watanabe, O.: Northern Hemisphere Forcing of Climatic Cycles in Antarctica over the Past 360,000 Years, Nature, 448, 912–916, https://doi.org/10.1038/nature06015, 2007.

Keller, K. M., Lienert, S., Bozbiyik, A., Stocker, T. F., Churakova (Sidorova), O. V., Frank, D. C., Klesse, S., Koven, C. D., Leuenberger, M., Riley, W. J., Saurer, M., Siegwolf, R., Weigt, R. B., and Joos, F.: 20th century changes in carbon isotopes and water-use efficiency: tree-ring-based evaluation of the CLM4.5 and LPX-Bern models, Biogeosciences, 14, 2641–2673, https://doi.org/https://doi.org/10.5194/bg-14-2641-2017, https://www.biogeosciences.net/14/2641/2017/, publisher: Copernicus GmbH, 2017.

Key, R. M., Kozyr, A., Sabine, C. L., Lee, K., Wanninkhof, R., Bullister, J. L., Feely, R. A., Millero, F. J., Mordy, C., and Peng, T.-H.: A Global Ocean Carbon Climatology: Results from Global Data Analysis Project (GLODAP), Global Biogeochemical Cycles, 18, https://doi.org/10.1029/2004GB002247, 2004.

Kleinen, T., Brovkin, V., and Schuldt, R. J.: A Dynamic Model of Wetland Extent and Peat Accumulation: Results for the Holocene, Biogeosciences, 9, 235–248, https://doi.org/https://doi.org/10.5194/bg-9-235-2012, 2012.

Kohn, M. J.: Carbon Isotope Compositions of Terrestrial C3 Plants as Indicators of (Paleo)Ecology and (Paleo)Climate, Proceedings of the National Academy of Sciences, 107, 19691–19695, https://doi.org/10.1073/pnas.1004933107, 2010.

Kopp, R. E., Simons, F. J., Mitrovica, J. X., Maloof, A. C., and Oppenheimer, M.: Probabilistic Assessment of Sea Level during the Last Interglacial Stage, Nature, 462, 863–867, https://doi.org/10.1038/nature08686, 2009.

Labeyrie, L. D., Leclaire, H., Waelbroeck, C., Cortijo, E., Duplessy, J.-C., Vidal, L., Elliot, M., and Le Coat, B.: Foraminiferal Stable Isotopes of Sediment Core CH69-K09, https://doi.org/https://doi.org/10.1594/PANGAEA.881464, 2017.

Landais, A., Masson-Delmotte, V., Capron, E., Langebroek, P. M., Bakker, P., Stone, E. J., Merz, N., Raible, C. C., Fischer, H., Orsi, A., Prié, F., Vinther, B., and Dahl-Jensen, D.: How Warm Was Greenland during the Last Interglacial Period?, Climate of the Past, 12, 1933–1948, https://doi.org/https://doi.org/10.5194/cp-12-1933-2016, 2016.

Larrasoaña, J. C., Roberts, A. P., and Rohling, E. J.: Dynamics of Green Sahara Periods and Their Role in Hominin Evolution, PLOS ONE, 8, e76514, https://doi.org/10.1371/journal.pone.0076514, 2013.

Laskar, J., Robutel, P., Joutel, F., Gastineau, M., Correia, A. C. M., and Levrard, B.: A Long-Term Numerical Solution for the Insolation Quantities of the Earth, Astronomy & Astrophysics, 428, 261–285, https://doi.org/10.1051/0004-6361:20041335, 2004.

Leavitt, S. W.: Systematics of Stable-Carbon Isotopic Differences between Gymnosperm and Angiosperm Trees, Plant Physiol. (Life Sci. Adv.), 11, 257–262, 1992.

Lehman, S. J., Sachs, J. P., Crotwell, A. M., Keigwin, L. D., and Boyle, E. A.: Relation of Subtropical Atlantic Temperature, High-Latitude
Ice Rafting, Deep Water Formation, and European Climate 130,000–60,000 Years Ago, Quaternary Science Reviews, 21, 1917–1924,
https://doi.org/10.1016/S0277-3791(02)00078-1, 2002.

485 Lisiecki, L. E. and Raymo, M. E.: A Pliocene-Pleistocene Stack of 57 Globally Distributed Benthic δ^{18}O Records, Paleoceanography, 20,
PA1003, https://doi.org/10.1029/2004PA001071, 2005.

Lisiecki, L. E. and Stern, J. V.: Regional and Global Benthic δ^{18}O Stacks for the Last Glacial Cycle, Paleoceanography, 31, 2016PA003 002,
https://doi.org/10.1002/2016PA003002, 2016.

Lototskaya, A. and Ganssen, G. M.: The Structure of Termination II (Penultimate Deglaciation and Eemian) in the North Atlantic, Quaternary
490 Science Reviews, 18, 1641–1654, https://doi.org/10.1016/S0277-3791(99)00011-6, 1999.

Lüthi, D., Le Floch, M., Bereiter, B., Blunier, T., Barnola, J.-M., Siegenthaler, U., Raynaud, D., Jouzel, J., Fischer, H., Kawamura, K., and
Stocker, T. F.: High-Resolution Carbon Dioxide Concentration Record 650,000–800,000 Years before Present, Nature, 453, 379–382,
https://doi.org/10.1038/nature06949, 2008.

Lynch-Stieglitz, J., Stocker, T. F., Broecker, W. S., and Fairbanks, R. G.: The Influence of Air-Sea Exchange on the Isotopic Composition of
495 Oceanic Carbon: Observations and Modeling, Global Biogeochemical Cycles, 9, 653–665, https://doi.org/10.1029/95GB02574, 1995.

Marcott, S. A., Shakun, J. D., Clark, P. U., and Mix, A. C.: A Reconstruction of Regional and Global Temperature for the Past 11,300 Years,
Science, 339, 1198–1201, https://doi.org/10.1126/science.1228026, 2013.

Martrat, B., Grimalt, J. O., López-Martinez, C., Cacho, I., Sierro, F. J., Flores, J.-A., Zahn, R., Canals, M., Curtis, J. H., and Hodell, D. A.:
Sea Surface Temperatures, Alkenones and Sedimentation Rate from ODP Hole 161-977A, https://doi.org/10.1594/PANGAEA.787811,
500 2004.

Masson-Delmotte, V., Stenni, B., Pol, K., Braconnot, P., Cattani, O., Falourd, S., Kageyama, M., Jouzel, J., Landais, A., Minster, B., Barnola,
J. M., Chappellaz, J., Krinner, G., Johnsen, S., Röthlisberger, R., Hansen, J., Mikolajewicz, U., and Otto-Bliesner, B.: EPICA Dome C
Record of Glacial and Interglacial Intensities, Quaternary Science Reviews, 29, 113–128, https://doi.org/10.1016/j.quascirev.2009.09.030,
2010.

505 Masson-Delmotte, V., Schulz, M., Abe-Ouchi, A., Beer, J., Ganopolski, J., González Rouco, J. F., Jansen, E., Lambeck, K., Luterbacher,
J., Naish, T., Osborn, T., Otto-Bliesner, B., Quinn, T., Ramesh, R., Rojas, M., Shao, X., and Timmermann, A.: Information from Pa-
leoclimate Archives, in: Climate Change 2013: The Physical Science Basis. Contribution of Working Group I to the Fifth Assess-
ment Report of the Intergovernmental Panel on Climate Change, edited by Stocker, T. F., Qin, D., Plattner, G.-K., Tignor, M., Allen,
S. K., Doschung, J., Nauels, A., Xia, Y., Bex, V., and Midgley, P. M., pp. 383–464, Cambridge University Press, Cambridge, UK,
510 https://doi.org/10.1017/CBO9781107415324.013, 2013.

McKay, N. P., Overpeck, J. T., and Otto-Bliesner, B. L.: The Role of Ocean Thermal Expansion in Last Interglacial Sea Level Rise, Geo-
physical Research Letters, 38, https://doi.org/10.1029/2011GL048280, 2011.

Menviel, L. and Joos, F.: Toward Explaining the Holocene Carbon Dioxide and Carbon Isotope Records: Results from Transient Ocean
Carbon Cycle-Climate Simulations, Paleoceanography, 27, https://doi.org/10.1029/2011PA002224, 2012.

515 Menviel, L., Mouchet, A., J. Meissner, K., Joos, F., and H. England, M.: Impact of Oceanic Circulation Changes on Atmospheric $\delta^{13}CO_2$,
Global Biogeochemical Cycles, 29, 1944–1961, https://doi.org/10.1002/2015GB005207, 2015.

Menviel, L., Yu, J., Joos, F., Mouchet, A., Meissner, K. J., and England, M. H.: Poorly Ventilated Deep Ocean at the Last Glacial Maximum
Inferred from Carbon Isotopes: A Data-Model Comparison Study, Paleoceanography, 32, 2–17, https://doi.org/10.1002/2016PA003024,
2017.

520 Menviel, L., Capron, E., Govin, A., Dutton, A., Tarasov, L., Abe-Ouchi, A., Drysdale, R. N., Gibbard, P. L., Gregoire, L., He, F., Ivanovic, R. F., Kageyama, M., Kawamura, K., Landais, A., Otto-Bliesner, B. L., Oyabu, I., Tzedakis, P. C., Wolff, E., and Zhang, X.: The Penultimate Deglaciation: Protocol for Paleoclimate Modelling Intercomparison Project (PMIP) Phase 4 Transient Numerical Simulations between 140 and 127 Ka, Version 1.0, Geoscientific Model Development, 12, 3649–3685, https://doi.org/https://doi.org/10.5194/gmd-12-3649-2019, 2019.

525 Mokeddem, Z., McManus, J. F., and Oppo, D. W.: Oceanographic Dynamics and the End of the Last Interglacial in the Subpolar North Atlantic, Proceedings of the National Academy of Sciences, 111, 11 263–11 268, https://doi.org/10.1073/pnas.1322103111, 2014.

Montero-Serrano, J.-C., Bout-Roumazeilles, V., Carlson, A. E., Tribovillard, N., Bory, A., Meunier, G., Sionneau, T., Flower, B. P., Martinez, P., Billy, I., and Riboulleau, A.: Contrasting Rainfall Patterns over North America during the Holocene and Last Interglacial as Recorded by Sediments of the Northern Gulf of Mexico, Geophysical Research Letters, 38, https://doi.org/10.1029/2011GL048194, 2011.

530 Muhs, D. R., Ager, T. A., and Begét, J. E.: Vegetation and Paleoclimate of the Last Interglacial Period, Central Alaska, Quaternary Science Reviews, 20, 41–61, https://doi.org/10.1016/S0277-3791(00)00132-3, 2001.

Novák, M., Buzek, F., and Adamová, M.: Vertical Trends in d13C, d15N and d34S Ratios in Bulk Sphagnum Peat, Soil Biology and Biochemistry, 31, 1343–1346, 1999.

Oliver, K. I. C., Hoogakker, B. A. A., Crowhurst, S., Henderson, G. M., Rickaby, R. E. M., Edwards, N. R., and Elderfield, H.: A Synthesis
535 of Marine Sediment Core δ^{13}C Data over the Last 150 000 Years, Climate of the Past, 5, 2497–2554, https://doi.org/10.5194/cpd-5-2497-2009, 2010.

Oppo, D. W., McManus, J. F., and Cullen, J. L.: Evolution and Demise of the Last Interglacial Warmth in the Subpolar North Atlantic, Quaternary Science Reviews, 25, 3268–3277, https://doi.org/10.1016/j.quascirev.2006.07.006, 2006.

Otto-Bliesner, B., Brady, E., Zhao, A., Brierley, C., Axford, Y., Capron, E., Govin, A., Hoffman, J., Isaacs, E., Kageyama, M., Scussolini, P.,
540 Tzedakis, P. C., Williams, C., Wolff, E., Abe-Ouchi, A., Braconnot, P., Ramos Buarque, S., Cao, J., de Vernal, A., Guarino, M. V., Guo, C., LeGrande, A. N., Lohmann, G., Meissner, K., Menviel, L., Nisancioglu, K., O'ishi, R., Salas Y Melia, D., Shi, X., Sicard, M., Sime, L., Tomas, R., Volodin, E., Yeung, N., Zhang, Q., Zhang, Z., and Zheng, W.: Large-Scale Features of Last Interglacial Climate: Results from Evaluating the Lig127k Simulations for CMIP6-PMIP4, Climate of the Past Discussions, https://doi.org/https://doi.org/10.5194/cp-2019-174, 2020.

545 Peterson, C. D., Lisiecki, L. E., and Stern, J. V.: Deglacial Whole-Ocean δ^{13}C Change Estimated from 480 Benthic Foraminiferal Records, Paleoceanography, 29, 549–563, https://doi.org/10.1002/2013PA002552, 2014.

Petit, J. R., Jouzel, J., Raynaud, D., Barkov, N. I., Barnola, J.-M., Basile, I., Bender, M., Chappellaz, J., Davis, M., Delaygue, G., Delmotte, M., Kotlyakov, V. M., Legrand, M., Lipenkov, V. Y., Lorius, C., Pépin, L., Ritz, C., Saltzman, E., and Stievenard, M.: Climate and Atmospheric History of the Past 420,000 Years from the Vostok Ice Core, Antarctica, Nature, 399, 429–436, https://doi.org/10.1038/20859,
550 1999.

Plikk, A., Engels, S., Luoto, T. P., Nazarova, L., Salonen, J. S., and Helmens, K. F.: Chironomid-Based Temperature Reconstruction for the Eemian Interglacial (MIS 5e) at Sokli, Northeast Finland, Journal of Paleolimnology, 61, 355–371, https://doi.org/10.1007/s10933-018-00064-y, 2019.

Poirier, R. K. and Billups, K.: The Intensification of Northern Component Deepwater Formation during the Mid-Pleistocene Climate Transi-
555 tion: Mid-Pleistocene Deep Water Circulation, Paleoceanography, 29, 1046–1061, https://doi.org/10.1002/2014PA002661, 2014.

Reyes, A. V., Froese, D. G., and Jensen, B. J. L.: Permafrost Response to Last Interglacial Warming: Field Evidence from Non-Glaciated Yukon and Alaska, Quaternary Science Reviews, 29, 3256–3274, https://doi.org/10.1016/j.quascirev.2010.07.013, 2010.

Rowe, P. J., Wickens, L. B., Sahy, D., Marca, A. D., Peckover, E., Noble, S., Özkul, M., Baykara, M. O., Millar, I. L., and Andrews, J. E.: Multi-Proxy Speleothem Record of Climate Instability during the Early Last Interglacial in Southern Turkey, Palaeogeography,

560   Palaeoclimatology, Palaeoecology, p. 109422, https://doi.org/10.1016/j.palaeo.2019.109422, 2019.

Sarmiento, J., Dunne, J., Gnanadesikan, A., Key, R., Matsumoto, K., and Slater, R.: A New Estimate of the $CaCO_3$ to Organic Carbon Export Ratio, Global Biogeochemical Cycles - GLOBAL BIOGEOCHEM CYCLE, 16, https://doi.org/10.1029/2002GB001919, 2002.

Schmittner, A., Gruber, N., Mix, A. C., Key, R. M., Tagliabue, A., and Westberry, T. K.: Biology and Air–Sea Gas Exchange Controls on the Distribution of Carbon Isotope Ratios (δ^{13}C) in the Ocean, Biogeosciences, 10, 5793–5816, https://doi.org/10.5194/bg-10-5793-2013,

565   2013.

Schneider, R., Schmitt, J., Köhler, P., Joos, F., and Fischer, H.: A Reconstruction of Atmospheric Carbon Dioxide and Its Stable Carbon Isotopic Composition from the Penultimate Glacial Maximum to the Last Glacial Inception, Clim. Past, 9, 2507–2523, https://doi.org/10.5194/cp-9-2507-2013, 2013.

Schubert, B. A. and Jahren, A. H.: The Effect of Atmospheric CO_2 Concentration on Carbon Isotope Fractionation in C3 Land Plants,

570   Geochimica et Cosmochimica Acta, 96, 29–43, https://doi.org/10.1016/j.gca.2012.08.003, 2012.

Schurgers, G., Mikolajewicz, U., Gröger, M., Maier-Reimer, E., Vizcaíno, M., and Winguth, A.: Dynamics of the Terrestrial Biosphere, Climate and Atmospheric CO_2 Concentration during Interglacials: A Comparison between Eemian and Holocene, Climate of the Past, 2, 205–220, https://doi.org/https://doi.org/10.5194/cp-2-205-2006, 2006.

Schuur, E. a. G., McGuire, A. D., Schädel, C., Grosse, G., Harden, J. W., Hayes, D. J., Hugelius, G., Koven, C. D., Kuhry, P., Lawrence,

575   D. M., Natali, S. M., Olefeldt, D., Romanovsky, V. E., Schaefer, K., Turetsky, M. R., Treat, C. C., and Vonk, J. E.: Climate Change and the Permafrost Carbon Feedback, Nature, 520, 171–179, https://doi.org/10.1038/nature14338, 2015.

Shackleton, N. J., Hall, M. A., and Vincent, E.: Phase Relationships between Millennial-Scale Events 64,000–24,000 Years Ago, Paleoceanography, 15, 565–569, https://doi.org/10.1029/2000PA000513, 2000.

Shackleton, S., Baggenstos, D., Menking, J. A., Dyonisius, M. N., Bereiter, B., Bauska, T. K., Rhodes, R. H., Brook, E. J., Petrenko, V. V.,

580   McConnell, J. R., Kellerhals, T., Häberli, M., Schmitt, J., Fischer, H., and Severinghaus, J. P.: Global Ocean Heat Content in the Last Interglacial, Nature Geoscience, 13, 77–81, https://doi.org/10.1038/s41561-019-0498-0, 2020.

Spahni, R., Chappellaz, J., Stocker, T. F., Loulergue, L., Hausammann, G., Kawamura, K., Flückiger, J., Schwander, J., Raynaud, D., Masson-Delmotte, V., and Jouzel, J.: Atmospheric Methane and Nitrous Oxide of the Late Pleistocene from Antarctic Ice Cores, Science, 310, 1317–1321, https://doi.org/10.1126/science.1120132, 2005.

585   Stapel, J. G., Schwamborn, G., Schirrmeister, L., Horsfield, B., and Mangelsdorf, K.: Substrate Potential of Last Interglacial to Holocene Permafrost Organic Matter for Future Microbial Greenhouse Gas Production, Biogeosciences, 15, 1969–1985, https://doi.org/https://doi.org/10.5194/bg-15-1969-2018, 2018.

Stein, R., Fahl, K., Gierz, P., Niessen, F., and Lohmann, G.: Arctic Ocean Sea Ice Cover during the Penultimate Glacial and the Last Interglacial, Nature Communications, 8, 373, https://doi.org/10.1038/s41467-017-00552-1, 2017.

590   Stern, J. V. and Lisiecki, L. E.: Termination 1 Timing in Radiocarbon-Dated Regional Benthic δ^{18}O Stacks, Paleoceanography, 29, 1127–1142, https://doi.org/10.1002/2014PA002700, 2014.

Tarasov, P., Granoszewski, W., Bezrukova, E., Brewer, S., Nita, M., Abzaeva, A., and Oberhänsli, H.: Quantitative Reconstruction of the Last Interglacial Vegetation and Climate Based on the Pollen Record from Lake Baikal, Russia, Climate Dynamics, 25, 625–637, https://doi.org/10.1007/s00382-005-0045-0, 2005.

595 Turetsky, M. R., Abbott, B. W., Jones, M. C., Anthony, K. W., Olefeldt, D., Schuur, E. A. G., Grosse, G., Kuhry, P., Hugelius, G., Koven, C., Lawrence, D. M., Gibson, C., Sannel, A. B. K., and McGuire, A. D.: Carbon Release through Abrupt Permafrost Thaw, Nature Geoscience, 13, 138–143, https://doi.org/10.1038/s41561-019-0526-0, 2020.

Tzedakis, P. C., Drysdale, R. N., Margari, V., Skinner, L. C., Menviel, L., Rhodes, R. H., Taschetto, A. S., Hodell, D. A., Crowhurst, S. J., Hellstrom, J. C., Fallick, A. E., Grimalt, J. O., McManus, J. F., Martrat, B., Mokeddem, Z., Parrenin, F., Regattieri, E., Roe,
600 K., and Zanchetta, G.: Enhanced Climate Instability in the North Atlantic and Southern Europe during the Last Interglacial, Nature Communications, 9, 1–14, https://doi.org/10.1038/s41467-018-06683-3, 2018.

Waelbroeck, C., Duplessy, J.-C., Michel, E., Labeyrie, L., Paillard, D., and Duprat, J.: The Timing of the Last Deglaciation in North Atlantic Climate Records, Nature, 412, 724–727, https://doi.org/10.1038/35089060, 2001.

Yu, Z., Loisel, J., Brosseau, D. P., Beilman, D. W., and Hunt, S. J.: Global Peatland Dynamics since the Last Glacial Maximum, Geophysical
605 Research Letters, 37, https://doi.org/10.1029/2010GL043584, 2010.

Zahn, R., Winn, K., and Sarnthein, M.: Benthic Foraminiferal $\delta13C$ and Accumulation Rates of Organic Carbon: Uvigerina Peregrina Group and Cibicidoides Wuellerstorfi, Paleoceanography, 1, 27–42, https://doi.org/10.1029/PA001i001p00027, 1986.

Zhang, J., Quay, P. D., and Wilbur, D. O.: Carbon Isotope Fractionation during Gas-Water Exchange and Dissolution of CO_2, Geochimica et Cosmochimica Acta, 59, 107–114, https://doi.org/10.1016/0016-7037(95)91550-D, 1995.